PROVIDING TECHNICAL AND ALGORITHMICAL SUPPORT TO THE PREDICTABLE PROPERTIES OF HONEYCOMB FILLER OBTAINED BY ADDITIVE PROCESSES

The object of this study is the FDM process underlying the 3D printing of thin-walled honeycomb-type shells. A solution to the problem of manufacturing a honeycomb filler for a sandwich panel or a panel as a whole, including a curved one, is based on the built model of the process parametric and functional reliability. To this end, the printer dynamics, the behavior of a non-rigid workpiece, and the peculiarities of filament feeding during printing have been analyzed in detail. It has been shown that the predicted mechanical properties, in particular, $[\sigma]_{x,y,z}$, are determined by the conditions of extrudate laying and the adhesive bonds formed between its elements, both in the laying plane and between layers, and depend directly on the laying density and on a number of dynamic and thermal phenomena occurring in the mating area. The layout density parameter ρ can be used as a factor in the strength characteristics of the finished article.

The application of rational conditions for the movement of the print head, certain features of the contour traversal, the use of supporting elements, and the correct positioning of the part on the printer's desktop allows for sufficiently reliable reproduction of cellular shell products with maximum strength.

It has been proven that the accuracy of basic dimensions of the designed structures corresponds to accuracy quality 11...12 according to engineering standards, which is acceptable for a wide range of applications. The wall thickness of the cellular elements is determined by the filament laying modes, which includes such parameters as extrusion speed, contour traversal speed and acceleration, extrusion temperature, and stacking pitch, but is not less than 1.5 times the diameter of the extruder nozzle. Such geometric parameters provide reasonable strength and rigidity for articles at operation while minimizing the weight of the honeycomb.

It has been established that cellular elements should be printed with the use of additional support means; at the same time, the latter do not exclude the occurrence of a certain number of defects whose evolution is not stable and whose presence must be taken into account when predicting the mechanical properties of the finished article

Keywords: mechanical characteristics and accuracy of 3-D printing, cellular systems, additive manufacturing defects, additive process reliability models

Oleksandr Salenko
Doctor of Technical Sciences, Professor*
Vasil Strutinsky
Doctor of Technical Sciences, Professor*
Konstantyn Avramov
Corresponding Member of the National Academy of Sciences of Ukraine, Doctor of Technical Sciences, Professor, Head of Department
Department of Nonlinear Mechanics and Mathematical Modeling
Anatolii Pidhornyi Institute of Power Machines and Systems of the National Academy of Sciences of Ukraine
Komunalnykiv str., 2/10, Kharkiv, Ukraine, 61046
Vadym Orel
Corresponding author
PhD
Department of Mechanical Engineering
Zhytomyr Polytechnic State University
Chudnivska str., 103, Zhytomyr, Ukraine, 10005
Dmytro Dzhulii
PhD*
Andrii Havrushkevych
PhD*
Anton Kostenko
Engineer
"FRONTLINE ROBOTICS" LLC
Nahirna str., 22, Kyiv, Ukraine, 04107
*Department of Machine Design
National Technical University of Ukraine
"Igor Sikorsky Kyiv Polytechnic Institute"
Beresteiskyi ave., 37, Kyiv, Ukraine, 03056

1. Introduction

Cellular systems are currently widely used in engineering practice. Sandwich panels, consisting of outer and inner shells with a cellular filler between them, have many applications [1], are used in aviation, astronautics, military equipment, as well as other assemblies. High design characteristics make such panels almost unique in cases where the use of other

materials is not possible, due to certain restrictions on force and temperature effects, vibration, ultraviolet exposure, and other harmful factors.

Cellular systems are made of both metallic and non-metallic materials (Fig. 1) [2, 3]; they can be hermetic or non-hermetic, with drainage holes. The presence of such holes makes it possible to equalize pressure when changing environmental conditions, which is important for aircraft. For spacecraft and satellites, depending on the purpose, cellular body elements can also be combined with heat pipes, which allows for a rational way to obtain the maximum weight gain of the supporting system of the device [4]. Current trends are highlighted in works that reflect successes in designing ultralight and high-strength thermal protection systems for spacecraft [5].
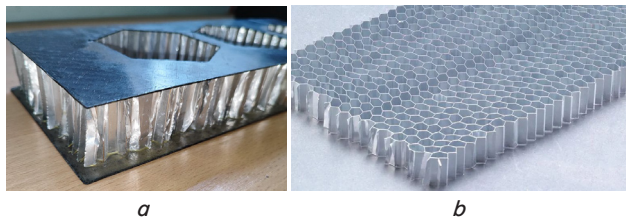

Fig. 1. Sandwich panels used in aerospace engineering: *a* — with metal elements; *b* — with non-metallic carbon-polymer sidewalls

Flat honeycomb systems of various technological purposes are shown in Fig. 2. Panels can have larger or smaller cell sizes, be strong and light, and have specific properties. The main advantages of using honeycombs in aircraft and spacecraft structures are high rigidity, reasonable strength, reliability, resistance to ultraviolet and X-ray radiation, etc. A significant disadvantage is the complexity of the structure and the high cost of honeycomb manufacturing process. Typically, designing honeycomb systems involves the preparation of two sidewalls (plates), the manufacture of honeycomb filler, its perforation, gluing (or welding) elements into a single system [6], as a result of which the cost of honeycomb panels remains quite high.
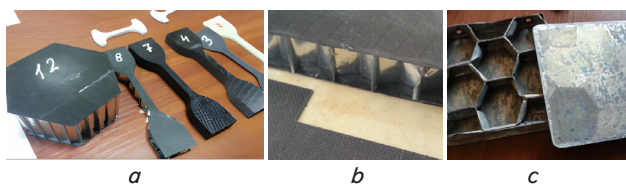

Fig. 2. Typical structure of sandwich panels: *a* — types of honeycomb panels; *b* — structural honeycomb with carbon sidewalls; *c* — heat-shielding heat-resistant honeycomb panel

There is experience in fabricating sandwich structures with honeycomb filling of a curvilinear shape [7]. Such technologies are used in small-class kamikaze drones, for which minimizing the cost of the supporting system plays a leading role. This is facilitated by the low rigidity of the honeycombs, the ability to impose it on surfaces of arbitrary shape [8].

Given the significant number of technological transitions, as well as the need to use special expensive equipment, honeycomb systems remain quite expensive, which limits their application in practice.

3-D printing technologies, the essence of which is to combine material particles into a finished article by controlled influence on the state of the material in microvolumes (for example, fusion, photopolymerization, sintering, etc.) according to certain algorithms, are a worthy alternative for manufacturing structures of complex shapes, including shell ones.

Therefore, it becomes obvious that the use of 3D printing tools accompanied by appropriate technologies could make it possible to design honeycombs of complex shapes and, as a result, to reduce the cost and expand the areas of sandwich panels application.

2. Literature review and problem statement

Paper [9] reports the results of studies that substantiate the prospects of forming cellular systems using additive technologies. It is shown that this approach makes it possible to partially overcome the shortcomings of conventional production methods and reduce the cost of the finished article; however, it does not take into account the defects that arise during the manufacturing process of an article using 3D printing and evolve later, as a result of which the mechanical properties of the finished article are quite low. Researchers focus on the use of affordable FDM printers or printers working with plastic filament [10] since this provides a lower cost of manufacturing cellular structures compared to panels manufactured in the conventional way.

There are also unresolved issues related to the limited efficiency of using more expensive technologies, in particular photopolymer printers [11] or laser selective melting units [12], which currently do not provide significant advantages for such tasks. A likely reason is both objective difficulties associated with the high cost of equipment and materials used in both technologies, and the inexpediency of using such technologies in view of the "price-quality" ratio.

An option for overcoming the difficulties of effective and stable defect-free printing is the application of combined solutions, in particular, printing with gradient [13] or paired heads [14], which makes it possible to form models using several types of filaments simultaneously. This approach has been used in a number of recent studies, in particular, [15], which also considers the mechanics of the behavior of shell systems made of combined materials under the action of thermobaric and concentrated loads.

In [16, 17], the authors paid attention to flat or axisymmetric honeycomb shells, while noting that the process of their additive reproduction faces a number of problems. In work [18], the researchers also noted that in most additive technologies there is a high probability of defects that negatively affect the operational properties of honeycomb articles. In addition, there are design restrictions on the thickness of honeycomb elements that are not typical for fillers made of metal foil [19]: for example, an attempt to build a thin wall that corresponds to the diameter of the extruder nozzle leads to a sharp decrease in the strength of an article, making it impossible to form it with increasing dimensions (mainly vertical), which requires the search for methods (algorithmic and technical) for the manufacture of thin-walled articles of complex configuration.

The problems of designing cylindrical shells were considered in [20, 21], in which it was proposed using a printer with a rotating cylindrical liner as a table for laying. This approach, despite the simplicity of implementation, makes it possible to obtain sufficiently high-quality honeycombs with fewer defects, however, the size of the honeycomb corresponds exclusively to the diameter of the table; other types of

honeycombs require the use of appropriate liner tables [22], which excludes the possibility of manufacturing a curved honeycomb of a non-axisymmetric shape. Therefore, this solution is specific and narrowly technological, which negates the advantages of additive processes.

Thus, despite the possibilities and obvious advantages of manufacturing honeycombs by additive processes, in particular FDM printing, there are a number of limiting factors, which involve the disparate information on defects arising during printing, their connection with the rigidity of the reproduced article, and the design features of printers, their adjustment: temperature regimes of laying, traceology, etc. The lack of such systematized information does not allow for the efficient and reliable manufacture of thin-walled shell molds, where incipient and developed defects significantly affect the mechanical properties of an article as a whole.

This gives us reason to argue that conducting research aimed at improving the process of manufacturing honeycomb fillers using FDM printing in order to reduce defects and predict the properties of an article as a whole could make it possible to systematize the knowledge about the causes of defects, to build process reliability models, and substantiate technical and algorithmic techniques to ensure stable mechanical characteristics of articles.

3. The aim and objectives of the study

The purpose of our study is to ensure the predicted properties of the cellular filler obtained by FDM printing by reducing the defect rate based on the constructed process reliability model, as well as by systematizing defects by their places of occurrence and further evolution. This will make it possible to employ FDM printing for the manufacture of cellular structures.

To achieve the goal, the following tasks were set:

– to conduct simulation modeling of the mechanical part of the printer in order to determine the main sources of dynamic positioning errors and, accordingly, the instability of conditions for connecting the extrudate fragments;

– to perform an analysis of the stress-strain state (SSS) of a workpiece and to investigate the influence of FDM printing modes, in particular, the density of filament laying and dynamic errors of the extruder movement on the predicted mechanical properties of articles;

– to clarify the systematization of defects formed during the reproduction of the part;

– to build and substantiate a mathematical model of the reliability of an FDM printing process of honeycomb fillers, to propose effective technical and algorithmic measures to improve the predictability of mechanical properties for a finished honeycomb item.

4. The study materials and methods

4. 1. The object and hypothesis of the study

The object of our study is the FDM process of 3D printing of thin-walled honeycomb shells.

The hypothesis of our study assumes the predictability of mechanical properties of honeycomb fillers manufactured by 3D printing, based on the establishment of regularities of filament laying in the dynamic system of the printer, taking into account the elastic properties of the workpiece of variable mass.

At the same time, it was assumed that the characteristics of strength and accuracy of an article depend on the types and number of defects that are formed during the formation of a thin wall. Since the article is reproduced in a dynamic system that includes the mechanical system of the printer and the part, as well as the phenomena of flow in the melt zone, extrusion, and subsequent solidification of the filament, it was decided to study the regularities in the formation of adhesive pads of the extrudate joints, since it was on them that the strength characteristics and accuracy indicators of the article depended.

It was also assumed that the formed defects, according to the theory of reliability of complex technical systems, in a certain way determine the parametric (less often – functional) reliability of the process; therefore, establishing the patterns of formation and evolution of defects could make it possible to identify a mathematical model of process reliability, determine the expected mechanical properties, and propose effective means for improving the reliability and predictability of an article as a whole.

4. 2. Theoretical data on predicting the emergence of defects during printing and determining the properties of cellular filler

Additive reproduction of cellular filler occurs by forming thin vertical connecting elements of flat or cylindrical shape (Fig. 3). Subsequently, plates are glued to such elements from above and below, thus forming cellular sandwich panels.
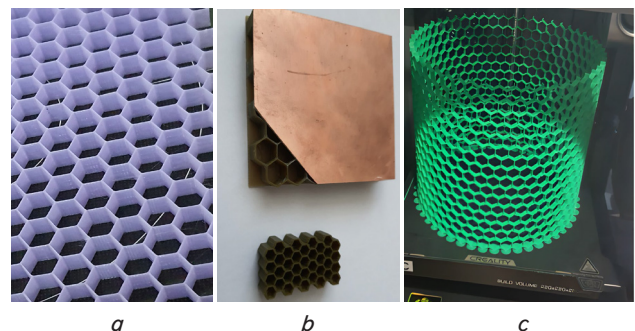

Fig. 3. Examples of cellular fillers: a — flat; b — as part of a sandwich panel; c — cylindrical

Certain improvements to the flat filament laying system and modification of control codes allow the fabrication of complex-profile articles, as noted by the authors of [17].

In addition to the above advantages, the use of additive processes, unlike existing technologies, allows for a gradient change in the parameters of honeycomb cells, it thereby provides variable mechanical characteristics: stiffness profiles, strength, etc.

Laying out a spatial non-rigid model by FDM printing is usually associated with a number of difficulties. This is evidenced by works [17, 23, 24], in which the authors analyze cases of disruption of the steady state of the technological process, which leads to the occurrence of a number of damages.

Considering the FDM printing process from the standpoint of reliability theory, it becomes obvious [19] that the reliability parameter is not a certain constant, an element of a matrix or a deterministic function, but is a mathematical expectation of the manifestation of a random variable within certain limits. Thus, each realization of the process $x_1(t)$, $x_2(t)...x_i(t)$, Fig. 4, a, is a function of time. It is known [25] that in the case when there are two boundaries described by curves

A and B, the formed strip will be the region of realization of the random process as a whole.

Since the set of realizations of a random process $x(t)$ for a fixed time instant t, which defines a certain cross-section, corresponds to a random variable represented by points (Fig. 4, b), a significant number N of realizations of a random process gives a set of random numbers that form a sample that characterizes the process as a function of time t [25]. This sample, represented graphically, is a set of points on the numerical axis x.
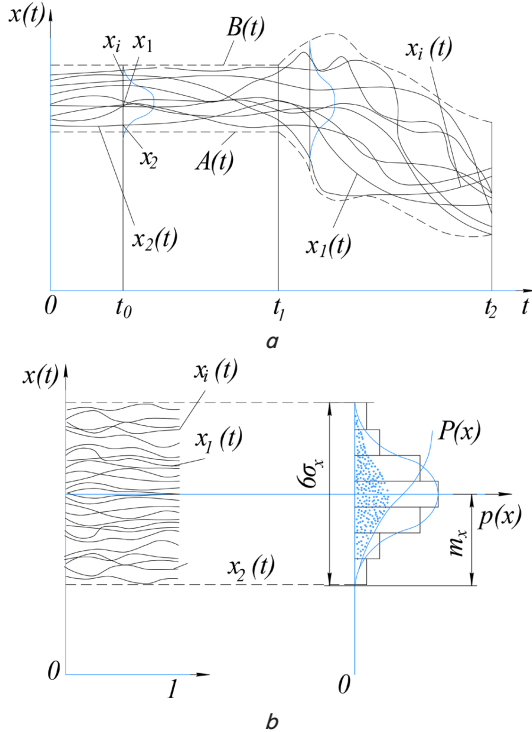
Fig. 4. An ensemble of realizations
of a random process: a — defined in the same time interval;
b — graphical interpretation of random values
of the process $x(t)$ in the section t with statistical
processing of the sample

The probability distribution function $P(x)$ for a Gaussian process is equal to the probability that the random process takes a value less than x. The probability that the random process $x^*(t)$ in the cross-section will fall into the interval between x_1 and x_2 is determined by the difference of the distribution functions

$$p(x_1 \leq x^*(t) < x_2) = P(x_1) - P(x_2). \qquad (1)$$

According to [26], the mathematical expectation of a random process in a cross section for a known probability density with an infinite number of realizations is determined by the dependence:

$$m_{2x}(t) = M[x^2(t)] = \int_{-\infty}^{+\infty} x^2 p(x)\mathrm{d}x, \qquad (2)$$

$$D_x(t) = \sigma_x^2(t) = M[(x(t) - m_x)^2]. \qquad (3)$$

Since [18] provides a fairly broad classification of defects, which reflects the nature of their occurrence, the mechanism of defect formation, its location, dimensions, etc., their totality

can be combined into certain groups. Based on our own research into the evolution of structural damage [16], such defects can be divided into groups according to their conditionality by the properties of the printer (mainly dynamic), printing modes, as well as the design of the reproduced model itself.

Then obtaining a cellular model of a given constant quality will be subject to that the normal course of the technological process provides for the following:

– no exceeding of the tolerance for the resulting size T_d, μm (both in the coordinates of the laying plane and vertically); absence of geometric errors of the contour elements, in particular, the predicted value of the thicknesses of the honeycomb walls (δ_{ci} with the specified parameters of the size dispersion;

– absence of violations of the conditions for the formation of adhesive adhesion, which can be conditionally determined by the strength characteristics (for example, tensile strength, σ_i) or by the relative elongation of the printed sample δ_i. This parameter, as well as the tensile strength σ_b, is functionally determined by the conditions of the adhesive contact formed during the connection of the layer following the main layer both in the interfilament and in the interplanar space;

– absence of conditions that lead to a change in the required volume of extrusion of the filament melt and form zones of under- or overextrusion, i.e., by the density of the extruded plastic stacking ρ_i, as well as by the mass of the manufactured samples m_s.

This condition is adequate, since under certain technological regimes (in particular, the speed of bypassing the contour s_k) it is possible to predict the strength parameters $[\sigma]_{x,y,z}$ with reasonable accuracy. Going beyond the established regimes will clearly mean the appearance of a defect and the need to re-manufacture the model.

Changing conditions or the manifestation of various violations of the steady progress of the technological process leads to the occurrence of both sudden and gradual failures in the system.

From these positions, the probability of a normal progress of the 3-D printing process can be as follows

$$P(t) = (1 - P_f(t)P_v(t)P_a(t)), \qquad (4)$$

where $P_v(t)$ is the probability of violation of the conditions for laying and solidification of the plastic, which assumes the exact location of the extruded filament in the laying plane above the previous thread; $P_f(t)$ is the probability of failures in the filament feed and the predicted volume of extrusion (violation of the conditions for extrusion and retract); $P_a(t)$ is the probability of violation of the conditions for adhesive adhesion to the base – the laying table.

The corresponding components of equation (4) can be obtained based on the analysis of the processes occurring in the system.

It was previously established that the destruction of structures formed by additive processes would occur with a simultaneous decrease in the fracture resistance of a quasi-cyclic nature, due to the evolution of initial defects on the adhesion planes and the development of such defects into microcracks that merge into main ones.

Taking into account [19], it can be stated that the shell 3-D article will lose its properties according to the gradual-sudden failure model, with damage increasing to catastrophic levels when the stresses reach critical values. Then the probability of failure-free operation of the shell article will be determined by the following model

$$P(T) = \left[0.5 + \Phi\left(\frac{H - H_a - \gamma_H T}{\sqrt{\sigma_H^2 + \sigma_\gamma^2 T}} \right) \right] e^{-\lambda T}, \qquad (5)$$

where $H = k\sigma$ is the ultimate strength, which determines the beginning of active crack formation; H_a – operational stresses, which are equivalent and include residual stresses (formed during plastic spreading) and working stresses (arising under the action of thermobaric loads p_b); γ_H – rate of change of equivalent stresses during the period of operation T; σ_H^2, σ_γ^2 – dispersion of actual values of strength (H) and speed γ_H; λ – failure rate (sudden). The speed γ_H is determined by the change in the rate of release of energy of elastic deformations (4), and parameters σ_H^2, σ_γ^2 – by the conditions of article formation (printing modes). The failure rate λ is empirical in nature and can be determined on the basis of a sample of statistical observations of parametric changes in the printing process.

This model is based on the features of the origin and evolution of defects in the article, which are directly determined by the conditions of its reproduction.

Therefore, by establishing regularities in the formation of initial defects and limiting the factors that lead to their emergence, we are able to ensure the predicted properties of the article, taking into account the degree of influence of technological printing parameters and adjust printing modes to achieve a given level of quality.

In general, the cause-and-effect diagram of the formation of initial quality indicators is shown in Fig. 5; the conditionality of initial quality indicators by the properties of the dynamic printer system and printing modes is given in Table 1.

Extrusion and joining of filament fragments into a single whole are directly determined by the dynamic properties of the printer: its ability to accurately move the extruder relative to the base surface, to allow dosage for extruding the filament, and provide the required thermobaric loading of the joining zone.
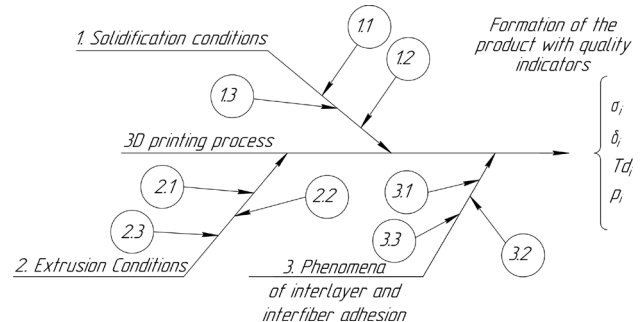

Fig. 5. Cause-and-effect diagram of the dependence of initial article properties on the printing modes and the dynamics of the printer used

The dynamic system of the printer can be represented as a multi-mass elastic system with an elastic-viscous connection of concentrated masses m_e, m_d, m_c with each other (in particular, using elastic links c_{npx}, c_{npy}); Fig. 6, a. Then, with multi-pass filament laying under reverse mode within the thickness of the honeycomb, the workpiece with mass m_d is such that it perceives a number of dynamic loads due to its own inertia F_i (Fig. 6, b) and the driving forces of the corresponding drives. The calculated models of the drive components are shown in Fig. 6, c. The concentrated masses are fed to the extruder m_1 and the horizontal movement frame m_2, which is connected to the vertical base beam on the vertical axis of the printer.

Table 1

Defects caused by the properties of the dynamic system of a 3-D printer

| Group	Defects	Properties of a dynamic system	Probability of violations
Group 1	D_1 – shrinkage	Chamber and table temperature conditions	$P_v(t)$ (solidification conditions)
		Layout density	
		Transfer speed, coordinated with extrusion speed	
	D_2 – deformation	Spreading density	
		Transfer speed matched with extrusion speed	
	D_4 – delamination	Temperature modes of the chamber and table	
	D_5 – twisting	Temperature modes of the chamber and table	
		Positioning	
	D_{11} – cracks	Layout density	$P_f(t)$ (extrusion conditions)
		Positioning	
		Filament properties	
Group 2	D_3 – shift	Extrusion speed and consistency	
		Transfer speed matched to extrusion speed	
	D_6 – gaps	Layout density	
		Positioning	
		Extrusion speed and consistency	
	D_7 – filaments outside	Positioning	$P_a(t)$ (adhesion)
		Movement speed matched with extrusion speed	
Group 3	D_8 – excessive extrusion	Laying density	
		Extrusion speed and consistency	
	D_9 – nedosextrusia	Extrusion speed and consistency	
	D_{10} – streaks	Laying density	
		Positioning	
	D_{12} – clots	Temperature conditions	
	D_{13} – voids	Temperature conditions	
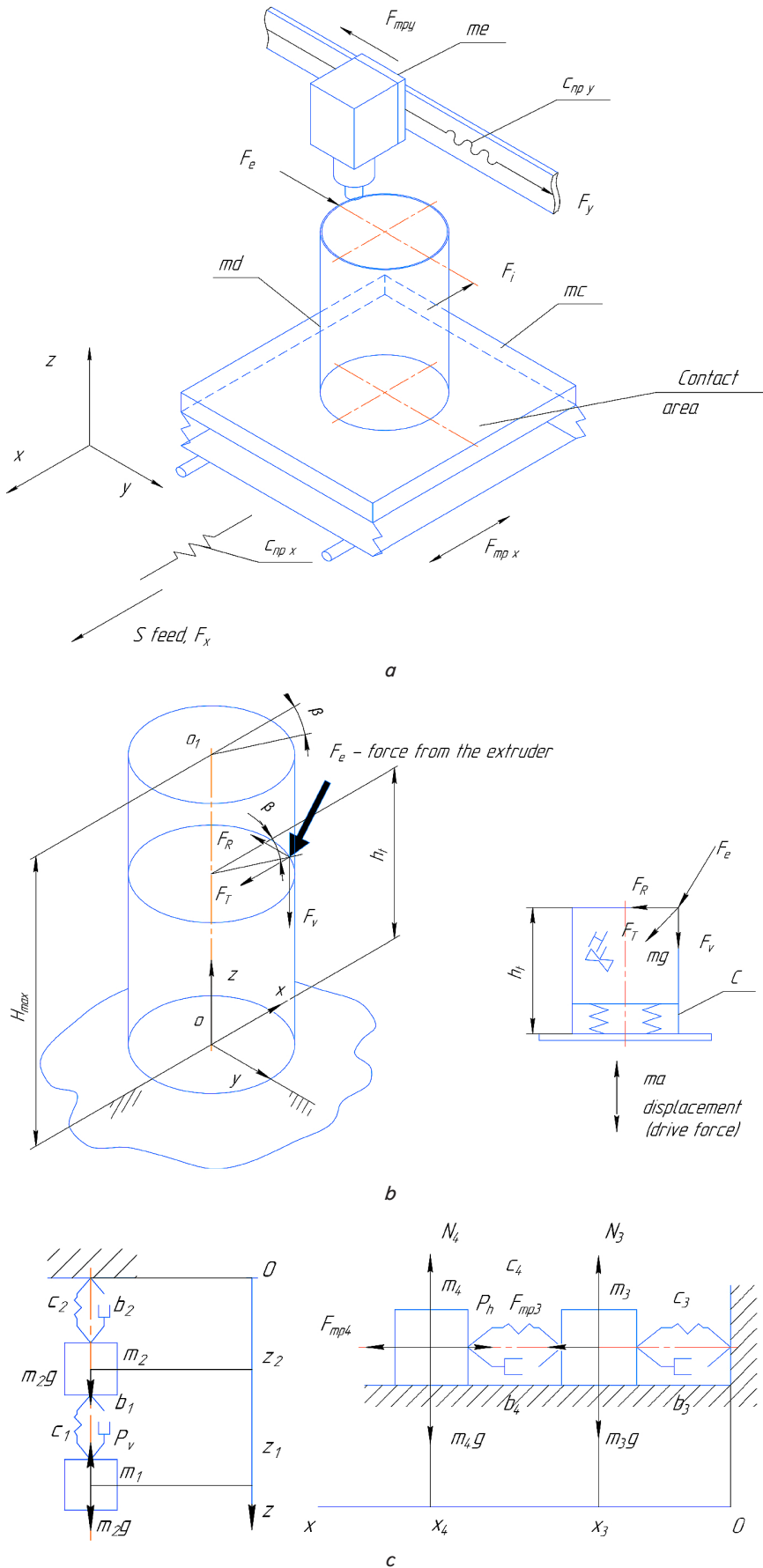
Fig. 6. Reproduction of the honeycomb model: a — vertical arrangement of the designed honeycomb; b — forces acting on the model; c — elastic dynamic models of the printer drive components for the vertical and horizontal axes

For the second module, the concentrated masses are brought to the elements of the horizontal support table m_3 and the finished article during its printing m_4, the connections between the connected masses are connections with limited rigidity, the mass of the printed object appears concentrated at a point.

In the case when a printer with X–Y core kinematics is used, the corresponding concentrated masses will be brought to other elements: now the vertical movement along the z coordinate will be carried out not by masses m_1 and m_2 but by masses m_3, m_4. Instead, masses m_1 and m_2 will carry out horizontal movement.

FDM printing involves extrusion in a state when a highly elastic plastic filament is formed by the nozzle, which, under the action of compression forces, elastic-plastic resistance, gravitational and friction forces, is pressed against the surface of the layout, Fig. 7, maintaining a certain temperature T_e during solidification time. As a result of the force action, the thread with a cross-section of diameter D_y changes its cross-section to a conditionally elliptical one with semi-axes $A/2$ and $B/2$, and a contact strip with a width of p_{i2} is formed on the reference plane. Displacing the extruder by step T_k and moving equidistant to the previous trajectory makes it possible to obtain a lateral contact strip, which is formed by "indenting" the material into the angle between the surface of the previous thread and the surface of the base.

Then the voidness will be determined by the ratio of the theoretical filling area of the layer gap $h_s k D_c$ to the cross-sectional area of the extruded filament $\pi AB/4$

$$\rho = \frac{\pi AB}{4h_s k D_c}, \tag{6}$$

h_s – layer thickness, mm; D_c – extruder nozzle diameter, mm; k – coefficient that takes into account the difference between the width of the extruded strip and nozzle diameter D_c.

The process reliability parameters associated with the phenomena of filament melt and its outflow from the nozzle are determined from the rheological equation for the filament melt (polymer thread) which, according to [10], takes the following form

$$\tau = K_1 e^{-\beta \frac{T-T_1}{T_1-273}} \cdot \gamma^n, \tag{7}$$

where β is the temperature coefficient, K_1 is the consistency coefficient (effective viscosity), t is the tangential stress. The yield curve for a polymer melt is $\tau = K\gamma^n$, where n is the power exponent, which characterizes the degree of non-Newtonian behavior of the melt and is the flow index. The coefficient K is a function of temperature, $Ke^{-\beta}$, so

$$\beta = -\frac{T_1}{T_2 - T_1} \ln\left(\frac{K_2}{K_1}\right). \tag{8}$$

Rheological parameters K and n are determined from experimental data according to [9]. The problem statement for establishing the influence of temperature phenomena in an invariant form includes kinematic relations, the equation of heat conductivity: $c_v\theta = \mathrm{div}(k\mathrm{grad}\theta) + Q$, quasi-static equilibrium: $\mathrm{div}\sigma = 0$, boundary and initial conditions: $\theta = \theta_0$ at $t = 0$; $-kn\cdot\mathrm{grad}\theta = -q + \gamma(\theta - \theta_c)$; $\sigma \times n = 0$. Here θ is the temperature; σ is the stress tensor; Q is the power of the volumetric heat source; q is the given heat flux; c_v and k are the coefficients of heat capacity and heat conductivity; γ is the heat transfer coefficient; θ_c is the ambient temperature; θ_0 is the initial temperature; n is the external normal to the body surface; $\sigma = (\sigma_{ij})$. $i, j = x, y, z$.
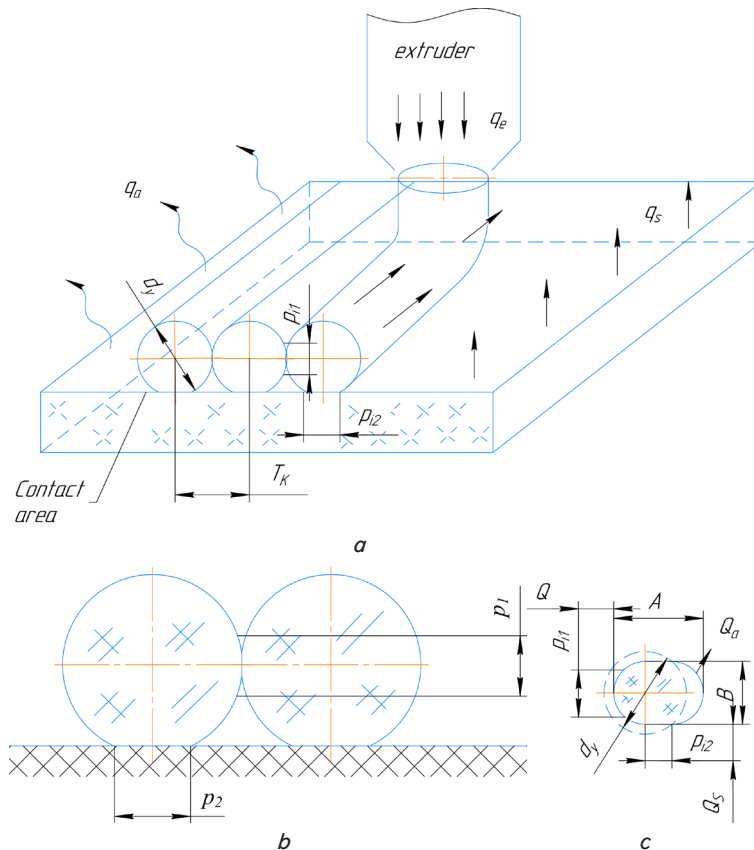
Fig. 7. Scheme of filament laying and formation of adhesion bands: a — general view; b — contact parameters of adjacent bands; c — basic parameters of a single band

Plane stress state in the OXY plane of the layout:

$$\sigma_{zz} = \sigma_{zx} = \sigma_{zy} = 0,\ u_i = u_i(x,y),$$

$$\varepsilon_{ij} = \varepsilon_{ij}(x,y),\ \sigma_{ij} = \sigma_{ij}(x,y),\ \theta = \theta(x,y). \tag{9}$$

The thermomechanical behavior of the material is described by the relations: $\varepsilon = \varepsilon^e + \varepsilon^\theta$; $e^\theta = \alpha(\theta - \theta_0)I$; $s = 2Ge$, $tr\sigma = 3K_v tr(\varepsilon - \varepsilon^\theta)$. Here ε^e and ε^θ are the elastic and thermal components of deformation, s and e are the deviators of the stress and strain tensors; G and K_v are the shear modulus and the bulk modulus; tr is the tensor trace; I is the unit tensor.

The reliability of constructing an engineering model is determined directly by the adhesion phenomena between the filaments and layers of extruded plastic; in this case, the conditions of the connection will be determined by the accuracy of the material laying. The latter is determined by the dynamics of the printer's supporting system and the deformability of the article during its laying.

The systems of differential equations of motion of concentrated masses for the vertical and horizontal systems of bodies of each analyzed module take the following form [25]. For a vertically moving link

$$\begin{cases} m_1 \cdot \dfrac{d^2 z_1}{dt^2} = m_1 g - F_b - c_1(z_1 - z_2) - \\[2mm] - b_1\left(\dfrac{dz_1}{dt} - \dfrac{dz_2}{dt}\right), \\[2mm] m_2 \cdot \dfrac{d^2 z_2}{dt^2} = m_2 g - c_2 z_2 - \\[2mm] - b_2\dfrac{dz_2}{dt} + c_1(z_1 - z_2) + b_1\left(\dfrac{dz_1}{dt} - \dfrac{dz_2}{dt}\right). \end{cases} \tag{10}$$

For a horizontal movable link:

$$\begin{cases} m_1 \cdot \dfrac{d^2 x_4}{dt^2} = -F_{er} - \mu \cdot m_1 g \cdot \mathrm{sgn}\left(\dfrac{dx_4}{dt}\right) - \\[2mm] - c_3(x_4 - x_3) - b_3\left(\dfrac{dx_4}{dt} - \dfrac{dx_3}{dt}\right), \\[2mm] m_2 \cdot \dfrac{d^2 x_3}{dt^2} = -\mu \cdot m_2 g \cdot \mathrm{sgn}\left(\dfrac{dx_3}{dt}\right) - \\[2mm] - c_3 x_3 - b_3\dfrac{dx_3}{dt} + c_4(x_4 - x_3) + \\[2mm] + b_3\left(\dfrac{dx_4}{dt} - \dfrac{dx_3}{dt}\right), \end{cases} \tag{11}$$

$$\begin{cases} m_3 \cdot \dfrac{d^2 x_5}{dt^2} = -R_{et} - \mu \cdot m_3 g \cdot \mathrm{sgn}\left(\dfrac{dx_5}{dt}\right) - \\[2mm] - c_5(x_6 - x_5) - b_5\left(\dfrac{dx_6}{dt} - \dfrac{dx_5}{dt}\right), \\[2mm] m_4 \cdot \dfrac{d^2 x_6}{dt^2} = -\mu \cdot m_4 g \cdot \mathrm{sgn}\left(\dfrac{dx_6}{dt}\right) - \\[2mm] - c_6 x_3 - b_6\dfrac{dx_6}{dt} + c_5(x_6 - x_5) + \\[2mm] + b_5\left(\dfrac{dx_6}{dt} - \dfrac{dx_5}{dt}\right). \end{cases} \tag{12}$$

The solution to equations (10) to (12) makes it possible to determine z_1, $z_2 = f(t)$; dz_1/dt, $dz_2/dt = f(t)$; x_3, $x_4 = f(t)$; dx_3/dt, $dx_4/dt = f(t)$; x_5, $x_6 = f(t)$; dx_5/dt, $dx_6/dt = f(t)$ taking into account that mass $m_4 = m_c + m_d$, and $m_2 = m_e + m_p$.

The system of differential equations was solved in the MATLAB Simulink environment; the values of the stiffness and dissipation parameters were previously determined, and the deviation δ_Σ of the coordinate of the output link at time t was indicated, i.e., $\delta_\Sigma(t) = \sqrt{x_6^2 + x_4^2}$, $x_4 = f(t)$; $x_6 = f(t)$.

Such a deviation will cause an inertial load on the non-rigid honeycomb structure with mass m_d, Fig. 8, as a result of which it becomes possible to estimate the displacements of the honeycomb top from the predicted point, which leads to the formation of errors in filament laying.
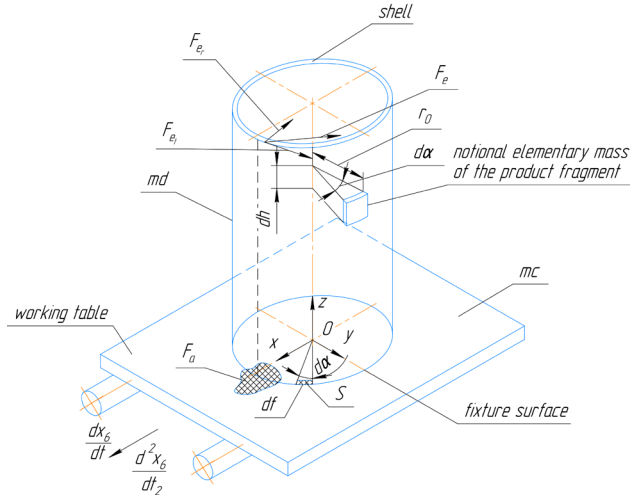

Fig. 8. Fixing the article with mass m_d on the workbench and force loading of the article during its reproduction

As the built model grows, its height H increases, Fig. 6, b, and mass m_d increases with an increase in its deformability from the force load.

Under certain circumstances, there comes a moment when the conditions for ensuring the density of laying ρ or strength σ_b become less than the required values, which, based on (4), will lead to parametric failure of the process.

The component geometric error of the formation of the adhesion contact plane is defined as follows

$$\chi = \sqrt{\delta_x^2 + \delta_y^2 + \eta^2} - \frac{kD_c}{2}, \qquad (13)$$

where δ_x is the drive error along the x coordinate; δ_y is the drive error along the y coordinate; η is the error from the action of the print head retractor; D_c is the diameter of the extrudate; k is a coefficient that takes into account the increase in the contact area when forming a strip with a variable width. In the general case for any printer systems, $\chi = f\delta_\Sigma$.

The errors δ_x and δ_y were determined based on mathematical modeling of the dynamic system according to the scheme in Fig. 6 and equations (10) to (12).

The decrease in the boundary values $[\sigma]_{x,y,z}$ will occur whenever the area of adhesive contact P between the filament threads and between the layers, Fig. 9, decreases.

Since the contact between the elements of the printed model (unlike the compact material) due to the compression of the previously cylindrical extrudate D_e to a conditionally elliptical one with semi-axes $A/2$ and $B/2$ and conditionality $\begin{cases} p_2 \leq T_k, D_e, \\ p_1 \leq h_s, D_e, \end{cases}$ occurs

through the strips p_2 and p_1, the

corresponding values of $[\sigma]_{x,y,z}$ must be reduced by value k_i, $[\sigma]_x = k_x\sigma_t$; $[\sigma]_y = k_y\sigma_t$; $[\sigma]_z = k_z\sigma_t$; $k_{x,y,z} = 0.35...0.85$ depending on the load application scheme (Fig. 9).
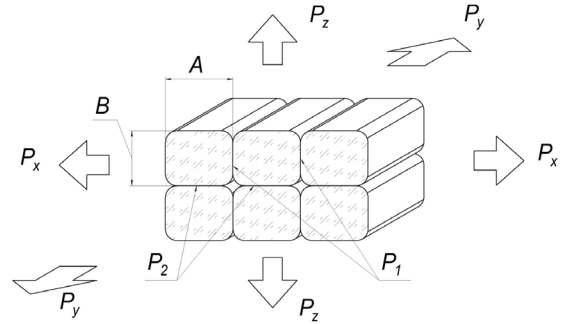

Fig. 9. Difference of adhesion areas in interfilament p_1 and interlayer p_2 spaces

4. 3. Methodology for manufacturing and testing the demonstrators of thin-walled shells obtained by FDM processes

Samples for engineering purposes are represented in the form of cellular cylindrical systems, the parametric model of which is shown in Fig. 10, provided that the dimensions of the manufacturing options are given in Table 2. Such a model was used as an internal insert of a cylindrical cellular tank.
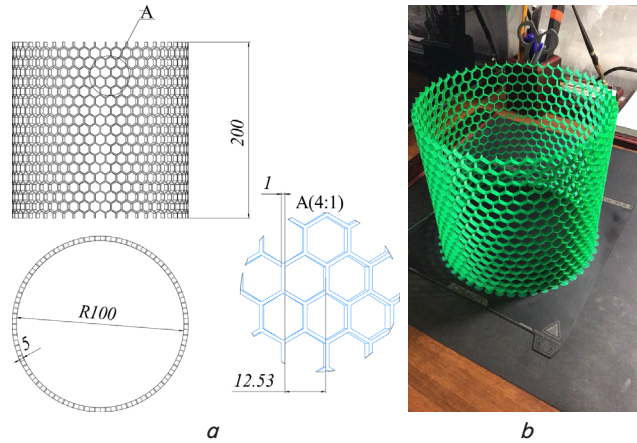

Fig. 10. Parametric model of the honeycomb shell:
a — with varied dimensions (diameter D_n, mm, honeycomb height h, mm, honeycomb cell pitch T, mm, and wall thickness δ, mm, and overall sample height H, mm); b — wall defects

Table 2

Dimensions of cylindrical cellular systems

No.	Honeycomb type	Honeycomb element settings				
		D_n, mm	h, mm	T, mm	δ, mm	H, mm
1	Test honeycomb with outer wall, PLA	160/158.5	10/10.6	12.5/11.9	1.0/1.15	40/41.1
2	Test honeycomb with inner wall, PLA	160/158.8	10/10.2	12.5/11.4	1.0/1.2	150/152.2
3	Test honeycomb without a wall, PLA	160/159.1	10/10.5	12.5/11.1	1.0/1.25	150/151.8
4	Reference honeycomb with an outer wall, PLA	200/200.8	6/6.3	12.5/11.9	0.5/0.65...0.7	200/201.8
5	Reference honeycomb without an outer wall, PLA	200/200.5	5/5.5	12.5/12.3	0.5/0.65...0.7	200/200.5
6	Reference honeycomb without an outer wall, PLA-C	200/201.1	5/5.4	12.5/12.1	0.5/0.58	200/200.9

Note: the numerator contains the specified value, the denominator contains the averaged measured value.

The stress-strain state of the workpiece during printing of the cellular element was determined in the SolidWorks environment (Dassault Systemes (France)), which is based on the calculation scheme in Fig. 6, *a*, *b*. The model in Fig. 9, *a* is rigidly fixed on the workbench, assuming that the model itself has finite rigidity and a distributed mass $m_4 = m_c + m_d = 0.32$ kg; the weight of the article itself, as will be taken into account later, is $m_d = 0.065...0.075$ kg.

Two types of plastics were used for printing – regular polylactide PLA (Fig. 11, *a*) and polylactide reinforced with carbon fiber PLA-CF (Fig. 11, *b*). The basic mechanical properties of the plastics are given in Table 3; printers' specifications with the basic technical characteristics are given in Table 4. The model was formed on the Creality Ender 3, Bambolab K1S, Creality K1C, JGAurora printers.

The first two printers have a classic layout with horizontal table movement (Bed Slinger) along the OY coordinate and a movable extrusion head in the vertical plane (OZ) and hori-zontal plane (OX). The latter printer works with vertical table movement (OZ) and head movement on two transverse horizontal rods XOY and implements Core XY kinematics.

a   *b*
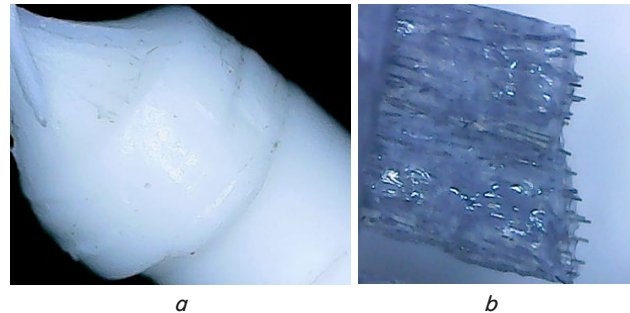
Fig. 11. Microphotographs of the filament produced by CREALITY: *a* — polylactide PLA; *b* — polylactide reinforced with carbon fiber PLA-CF

Table 3

Comparing the mechanical characteristics of filaments specified by the manufacturer with the experimental results of test samples

ID	Tensile strength, MPa		Young's modulus, MPa, $\times 10^3$		Impact strength, J/m³		Heat resistance, °C	
	Claimed	Test zraok	Claimed	Test zraok	Claimed	Test zraok	Claimed	Test zraok
PLA-C	59–63	58.4	1.68–1.96	1.65	66–92	74	59	65
PLA	28–32	33.1	1.2–1.3	1.24	53–135	90	76	82

Table 4

Technical specifications of the printers used

No.	Printer model and its characteristics	Printer photograph
1	Creality Ender 3. Printing technology: FDM. Print area: 220 × 220 × 240 mm. Printer dimensions: 433 × 366 × 490 mm. Weight: 7.8 kg. Typical print speed: up to 300 mm/s. The print speed for high quality is up to 100 mm/s. Max. print speed: 500 mm/s (test with Hyper PLA). Max. extruder motion acceleration: 8000 mm/s²	
2	JG Aurora. Number of extruders: one. Nozzle diameter: 0.4 mm. Nozzle temperature max: 240. Printing area: 205 × 205 × 205 mm. Layer thickness: 0.1–0.3 mm. Print speed: 10–100 mm/s (50–70 mm/s). Platform temperature: up to 110 °C. Materials: ABS, PLA, PETG. Material diameter: 1.75 mm. File format: G-code, OBJ, STL. Power supply: 180 W. Software: Cura	
3	Creality K1C. Number of print heads: 1. Print speed: up to 600 mm/s. Nozzle diameter: 0.4 mm. Construction area: 220 × 220 × 250 mm. Layer thickness: 0.1–0.35 mm. Maximum print speed: 600 mm/sec. Touch display: LCD display. Printing material: PA, PETG, PLA, TPU, PET, PLA-CF, PA-CF, PET-CF, PC, ASA, ABS. Thread diameter: 1.75 mm. Interfaces: Wi-Fi , SD card slot, USB. File types: STL, .obj, AMF. Compatible software: Cura, Creality Slicer, Simplify3D	

Since the layers are usually laid out with a thickness of 0.1 mm, a micrometer MK-0-10 with a digital division of 0.01 mm was used to measure the controlled values, which, owing to the flat ends of a significant plane, allows for more accurate determination of the average values of the controlled thicknesses. The surface profile when printing test samples was determined using a Mitutoyo Surftest SJ-210 profilometer.

To determine the density of the structure and defects in the filament stacking, an Opticon Biolife Pro optical microscope with a resolution of 5 μm (no worse) and a magnification of up to 800x was used.

The determination of strength parameters was performed on a model P-20 tensile testing machine. Special strain gauge devices were used to determine critical stresses.

Table 5 gives values of the stiffness, damping, and concentrated mass parameters for the Bed Slinger and Core XY printers. The reduced masses $m_1 - m_4$, kg, are selected from the three-dimensional assembly model in Solidworks, the stiffness values $c_1 - c_4$, N/m, and the damping coefficients $b_1 - b_4$, N·s/m, are accepted approximately for this type of printer.

Calculation of transient processes described by equations (10) to (12) and further modeling using Solid Works SSS with determination of displacements and deformations of elements of the studied system make it possible to determine the parameters of the formation zone of honeycomb elements and predict the indicators of strength and relative elongation of the finished part, as well as to identify the model of reliability of the process as a whole.

The application of acting forces, in particular F_e, was performed on the basis of the calculation schemes in Fig. 6, 8, despite the small value of the equivalent force F_e from the viscosity of the molten polymer components F_{er} and F_{et} (Fig. 8), (0.03...0.15 N) was taken into account, the model coefficient $k_m = 20$ was applied; the weight of the workpiece itself is assumed to be distributed over the surface, with a maximum value at full height $h = 0.2$ m $G = 1.25$ N. From below, the model is rigidly fixed on the worktable (despite the fact that in the previous analysis the connection between the table and the part was considered elastic, and the masses were concentrated), and the inertia forces are directed in the opposite direction from the movement.

It is also taken into account that the specified scheme is typical for Bed Slinger printers with a moving table; since in Core XY printers the table moved exclusively in a vertical plane, the dynamics of the extruder carriage were taken into account.

The angle β between the table motion vector OY and the extruder motion vector at a specific time point R (Fig. 6, b) was also taken into account, which, when they coincided, had the maximum force effect on the model.

5. Results of research on manufacturing a test honeycomb article with predicted properties

5. 1. Modeling the mechanical part of a 3D printer

Mathematical modeling of the dynamic system of a 3D printer for violation of rational conditions for the formation of adhesive contact areas according to Fig. 9 allowed us to obtain a number of the following generalizations (Fig. 12, 13). The module of vertical movement of the table is quite stable in operation since the movement speed is quite low, and the nonlinearity of friction forces can be neglected. The stepper motor with a helical gear has a sufficient degree of damping. Transient processes, Fig. 12, after changing the movement conditions cause short-term oscillations of small amplitude, which quickly decay.

The force F_b, which occurs during printing and is calculated on the basis of the arising stresses according to (9), is relatively small and can be neglected. The stability of the system remains satisfactory in the entire range of movements, speeds, and positions.

The transition to the calculation of horizontal coordinates and the consideration of nonlinear friction forces significantly changes the pattern of transient processes; Fig. 13. When the working body moves, the magnitude of the friction force does not change, but only the direction of action changes – unlike the direction of movement of the worktable or, in fact, the movement of the carriage by the guides. The components of the Creality Ender 3 printer are quite inertial, while the carriage of the Creality K1C printer is more rigid and less inertial.

Table 5

Dynamic parameters of models of multi-volume printer systems

Dynamic parameters of models Bed Slinger (Creality Ender 3, JG Aurora)			
Characteristics, measurement unit	Values	Characteristics, measurement unit	Values
m_1, kg	0.45	c_4, N/m	$4 \cdot 10^6$
m_2, kg	1.25	b_1, N·s/m	300
m_3, kg	0.5	b_2, N·s/m	600
m_4, kg	0.32	b_3, N·s/m	300
c_1, N/m	$2 \cdot 10^6$	b_4, N·s/m	600
c_2, N/m	$4 \cdot 10^6$	P_v, N	0.3
c_3, N/m	$2 \cdot 10^6$	P_h, N	0.1
Dynamic parameters of models Core XY (Creality K1C)			
Characteristics, measurement unit	Values	Characteristics, measurement unit	Values
m_1, kg	0.39	c_4, N/m	$4 \cdot 10^6$
m_2, kg	0.65	b_1, N·s/m	300
m_3, kg	0.9	b_2, N·s/m	600
m_4, kg	0.32	b_3, N·s/m	300
c_1, N/m	$2 \cdot 10^6$	b_4, N·s/m	600
c_2, N/m	$4 \cdot 10^6$	P_v, N	0.3
c_3, N/m	$2 \cdot 10^6$	P_h, N	0.1

Thus, the choice of the Core XY drive system (for example, printers such as Creality K1C) leads to an improvement in the dynamic properties of the entire system – a decrease in the frequency and amplitude of oscillations and is more desirable for printing thin, non-rigid parts. The use of braking algorithms in the working bodies at the end of the working stroke in coordination with the connected drives has a positive effect.

The use of the MATLAB Simulink package for modeling dynamic processes using the system of differential equations (10) to (12) allowed us not only to predict geometric errors in the reproduction of the model shape but also determine the conditions for the connection of layers and threads with each other.

In fact, any shifts at the contact boundary during extrusion lead to a change in the conditions for fusing the layers, which would determine the gaps and cavities in the designed structure (in particular, parameter ρ). On the other hand, non-density and changes in contact conditions can also cause a decrease in the strength characteristics σ_v, a change in the elastic moduli E and G and the coefficient of relative elongation δ.

a

b
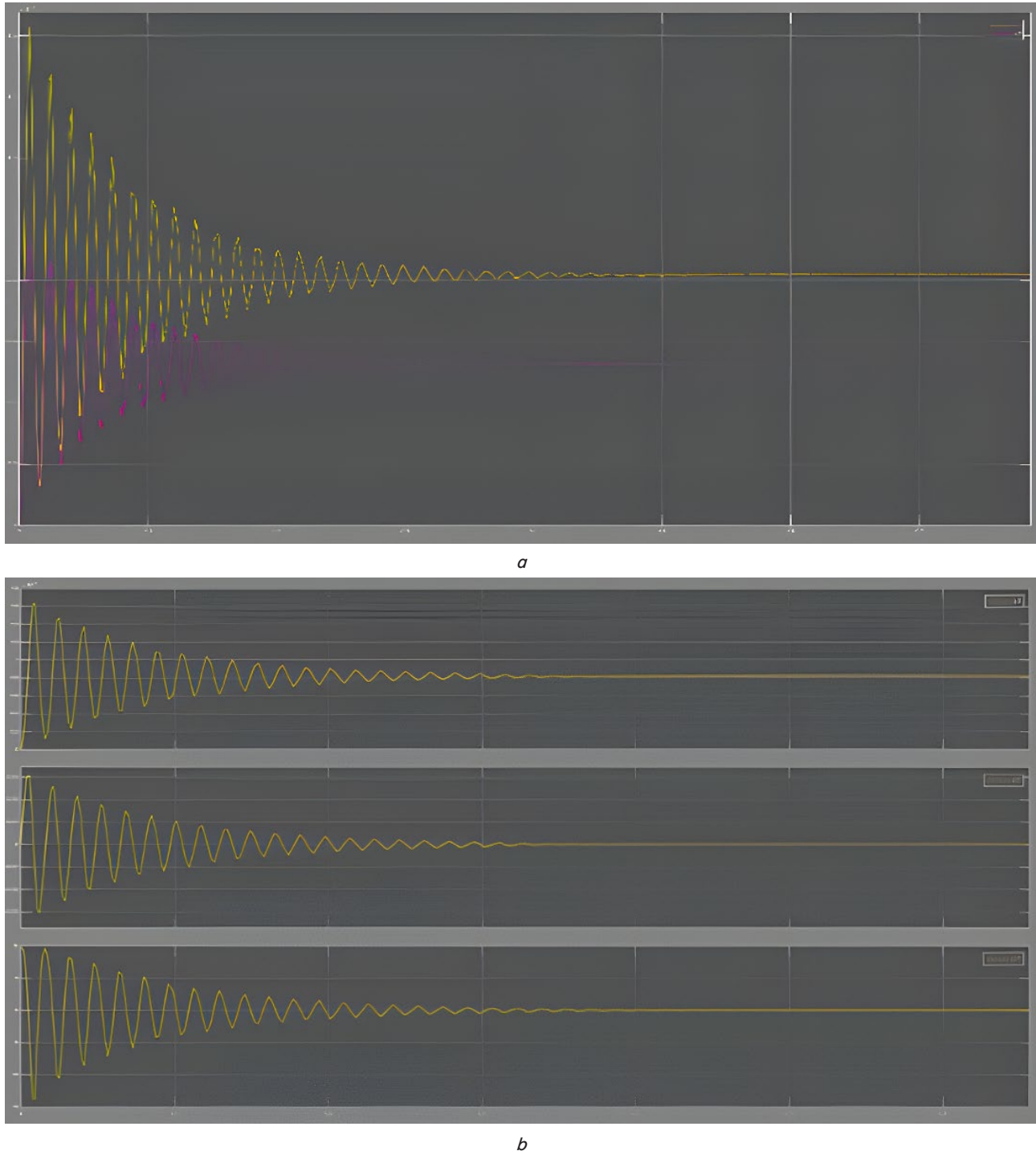
Fig. 12. Results of vertical module simulation: a — change in coordinates z_1 and z_2 during the oscillation damping period; b — values of the coordinate, velocity, and acceleration of the first body during the oscillation damping period

a

b
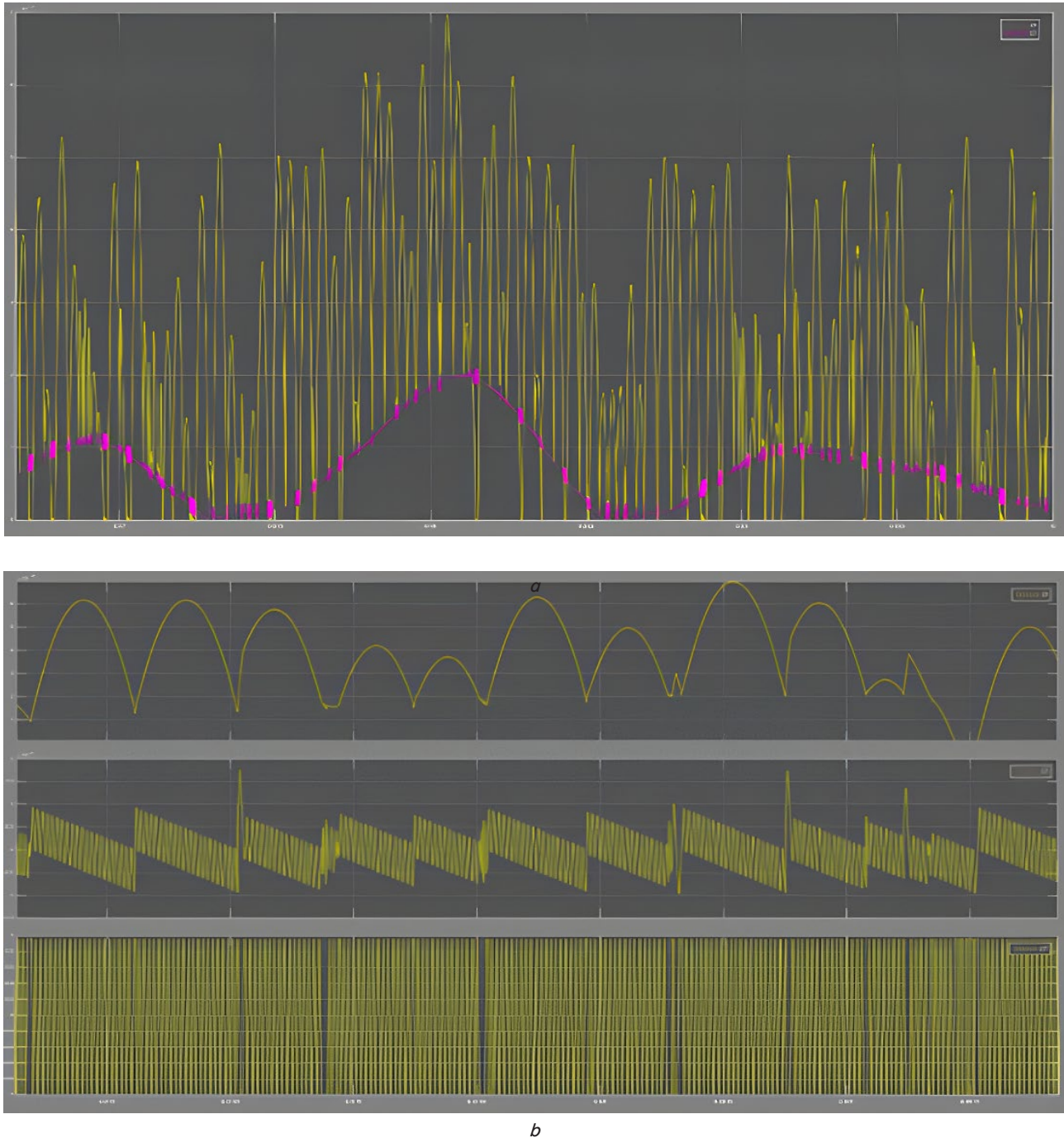
Fig. 13. Results of modeling the horizontal module: *a* — change in coordinates x_4 and x_6 during the period of oscillation damping; *b* — values of the coordinate, velocity, and acceleration of the workpiece installed on the table during the period of oscillation damping

5. 2. Analyzing the stress-strain state of an article in the process of 3-D printing

When analyzing SSS, the attention is focused on determining possible deviations δ from the rational conditions of theoretical contact of the filament emerging from the printing head with the laying base, which for this case was the plane of the previous bonding layer; Fig. 14. Thus, the deviation in the laying plane χ, (13), will lead to a reduction in the contact plane, Fig. 7, *b*, in the vertical one – to a change in the degree of pressing and to a change in the hollowness ρ, estimated by (5).

The model was generated based on the image in Fig. 9, *a*, the location on the workbench is vertical, the number of model elements is 40555, the size of the structural element is 13.3 mm, and the tolerance on the size is 0.46 mm; Table 6. The model is defined as linear elastic and isotropic, which makes it possible to analyze the action of inertial forces at significant accelerations of the working body.

As a result of our calculations, the stress distribution patterns in the honeycomb elements were obtained, Fig. 15, *a*, as well as deformations, Fig. 15, *b*, and displacements, Fig. 15, *c*. The calculations were performed for Core XY layout printers.

In this case, it was established, Fig. 15, *d*, that the stresses do not spread further than one layer of honeycombs (to a depth of 12…15 mm). The insignificant force F_e, which

is determined by the extrusion parameters (using (11)) at the filament extrusion speed, associated with the speed of bypassing the contour. At small cross-sections, it can create significant stresses (up to 12...18 MPa), which are critical for the material of the lower layers at the glass transition temperature ($T = 65...80$ °C) at the corresponding contact areas.

Fig. 16 shows a refined pattern of movements of the honeycomb elements at its maximum height $H = 200$ mm. The honeycomb itself is rotated relative to the central axis, and the force reaches its maximum value ($F_e = 0.15$ N).

It becomes obvious that such movements can be significant already over a larger area due to the low rigidity of the system. From the side of the extruder action at the maximum height (about $H = 200$ mm) the movements can reach 0.22...0.28 mm; however, at heights less than $H = 50...80$ mm, the movement becomes less than 0.1 mm.
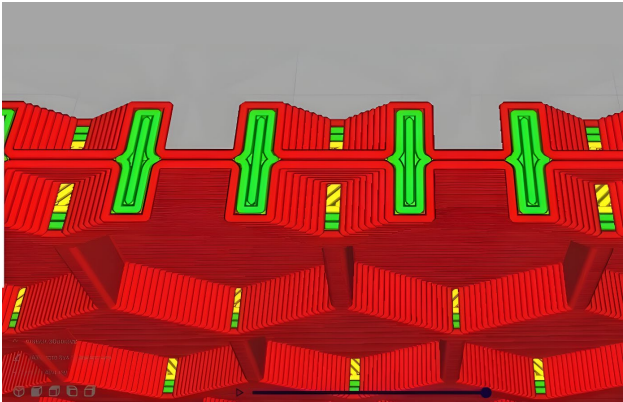
Fig. 14. Trasology of honeycomb construction and possible deviations of adhesion contact planes

Table 6

Information on dividing the honeycomb model

Mesh type	Solid mesh	Mesh quality	Draft
Mesher used	Standard mesh	Total nodes	14821
Automatic transition	Off	Total elements	40555
Include mesh auto loops	Off	Maximum aspect ratio	43.593
Jacobian points for high quality mesh	16 points	% of elements with aspect ratio < 3	2.91
Element size	13.3072 mm	Percentage of elements with aspect ratio > 10	26.1
Tolerance	0.466918 mm	Time to complete mesh (h; m; s):	00:03:01
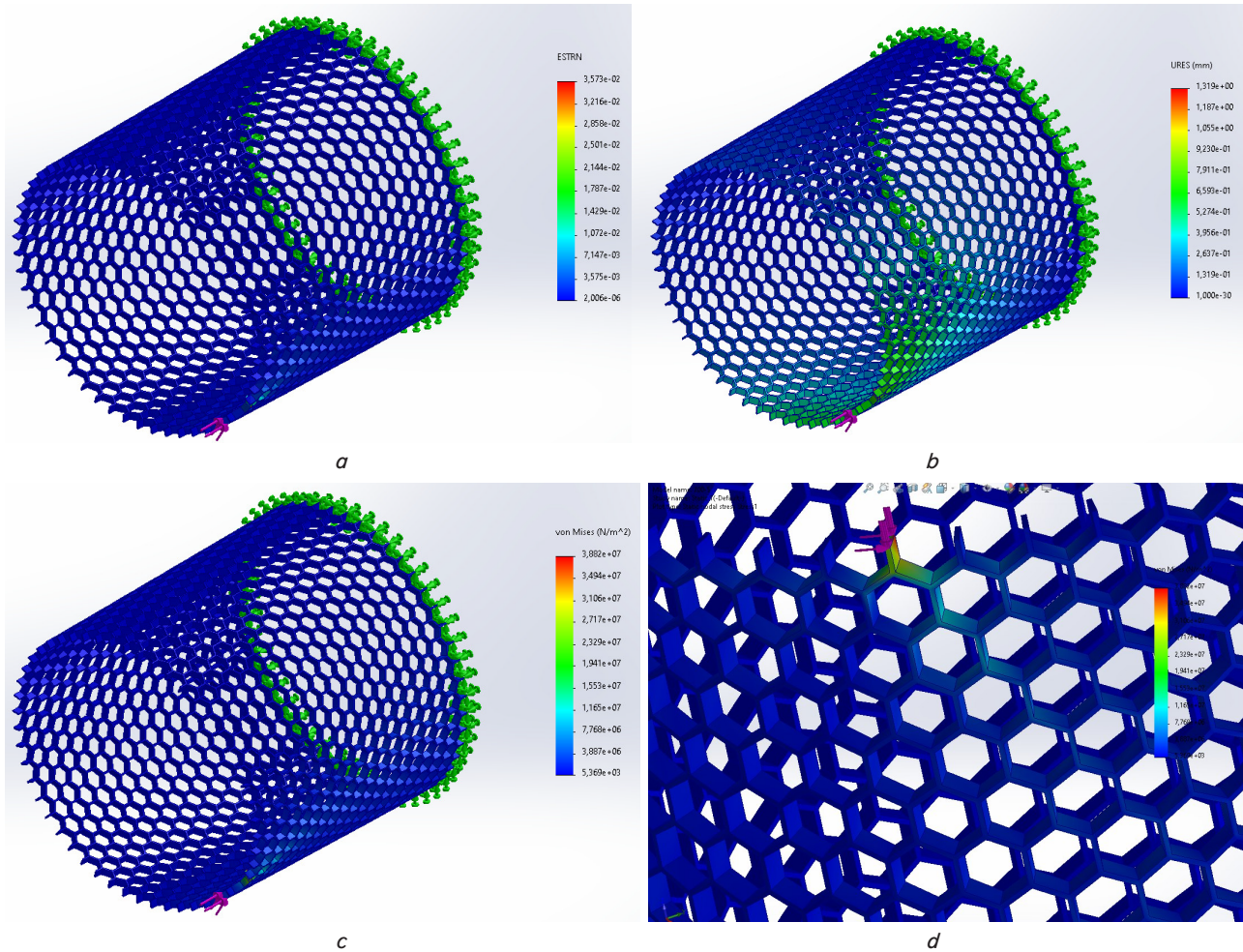
Fig. 15. Distribution of equivalent stresses in the elements of the honeycomb according to Mises:
a − deformations; *b* − displacements; *c* − with a stationary table; *d* − force action from the extruder
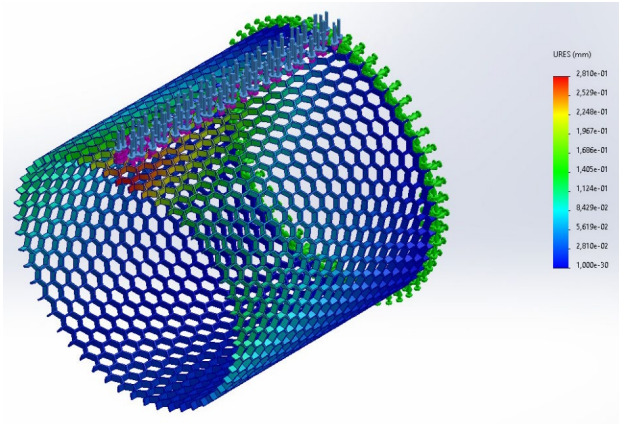
Fig. 16. Refined pattern of simulated displacements depending on the force effect of the extruder

In this case, the shape changes cover both the frontal part of the surface (from the side of the force) and the sides.

A distinctive pattern is observed when using a printer with a kinematic scheme with a moving worktable and a traverse (for Bed Slinger printer layouts). In this case, the acceleration of the table will cause the appearance of inertial forces F_i (Fig. 6) and, accordingly, significant deformations of the workpiece, especially in the case when the head is at a point on the line of movement of the table with maximum acceleration; Fig. 17.
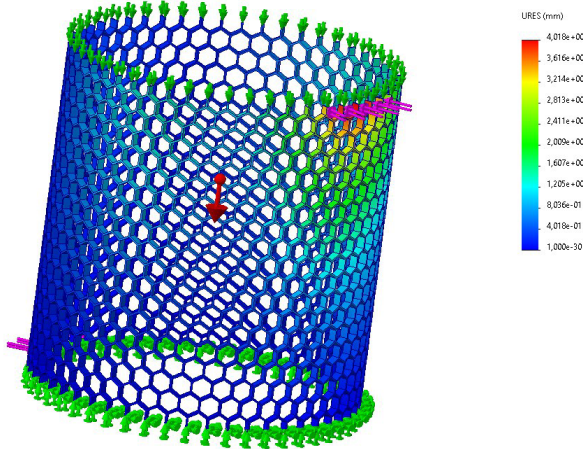
Fig. 17. Distribution of model element displacements due to inertial forces combined with force from the extruder

Different angles β (Fig. 6, b) revealed a distinct deformation of the walls of the non-rigid article and, accordingly, a distinct distribution of stresses on the surface of article fixation; Fig. 18.

As already noted, the stresses on the table area reach their maximum value at $\beta = 0$, at $\beta = \pi/4$ and $\beta = \pi/2$ the stresses decrease significantly and remain practically identical.

The errors on the laying area χ were estimated, which were determined by the difference between the expected position of the extruder and the modeled one, associated with the dynamic properties of the system. They directly determine the controlled parameters tensile strength, σ_i, and the relative elongation of the sample δ_i, which are functionally determined by the conditions of the adhesive contact (in particular, the area of contact f_a, the hollowness of article structures ρ, determined from (6)).

a

b

c
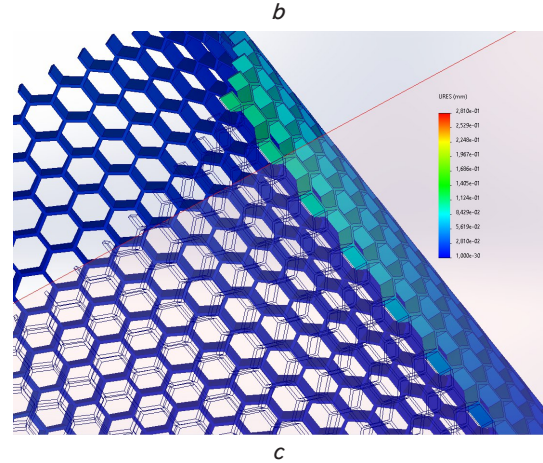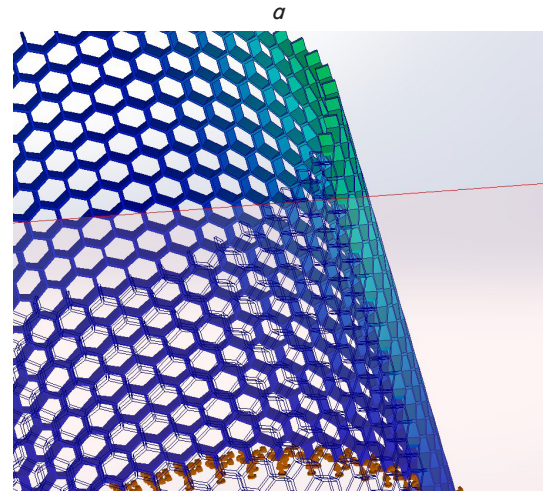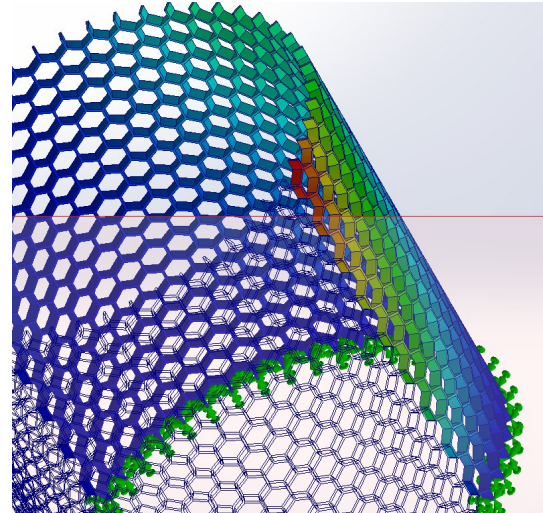
Fig. 18. Difference in the SSS of the honeycomb at different angles of force action of the extruder and taking into account the inertial components of Bed Slinger printers: $a - \beta = 0$; $b - \beta = \pi/4$; $c - \beta = \pi/2$

For this purpose, we established the dependence of error value χ, mm, on the contact planes on the distance of the laying area itself from the table surface, $\chi = f(H)$, as well as the error χ, mm, as a function of the laying speed (circumvention of the contour), $\chi = f(dy_6/dt)$. The modeling was carried out taking into account the capabilities of the printers used: for the Bed Slinger layout, the contour bypass speed was selected to be 35 mm/s, for the Core X-Y printer – 200 and 500 mm/s.

The results of statistical data processing in the Statgraphics Centurion environment are given in Table 7. According to the above analysis, it is not difficult to conclude that the error χ is affected by both the contour bypass speed S_k and the distance from table H when this is associated with the Bed Slinger system. Under such circumstances, the scatter fields of the values are quite wide, which does not allow us to obtain a clear regression dependence for predicting the quality of the finished article. At the same time, the influence of distance H from the table surface when printing the model, although increasing, has no statistical significance. All data during preliminary verification of statistical hypotheses can be attributed to one general population; thus, the regression dependence $\chi = 0.139 + 0.0029h$ is statistically insignificant, although a slight increase in the error, which manifests itself at a higher height of the corresponding table H, mm, is observed.

For fixed speeds of 200 mm/s and 500 mm/s, the corresponding regression equations for χ, mm, take the form:

$$\chi = 0.2 + 1.25 \cdot 10^{-3} h, \, v = 200 \text{ mm/s};\tag{14}$$

$$\chi = 0.3 + 2.3 \cdot 10^{-3} h, \, v = 500 \text{ mm/s}.\tag{15}$$

The influence of the speed of bypassing the contour S_k on error χ is generally satisfactorily described linearly by the dependence $\chi = f(v_6) = b_0 + b_1 s_k$, $\chi = 0.1177 - 0.1087 s_k$, $R^2 = 0.9726$, and takes the form shown in Fig. 19.
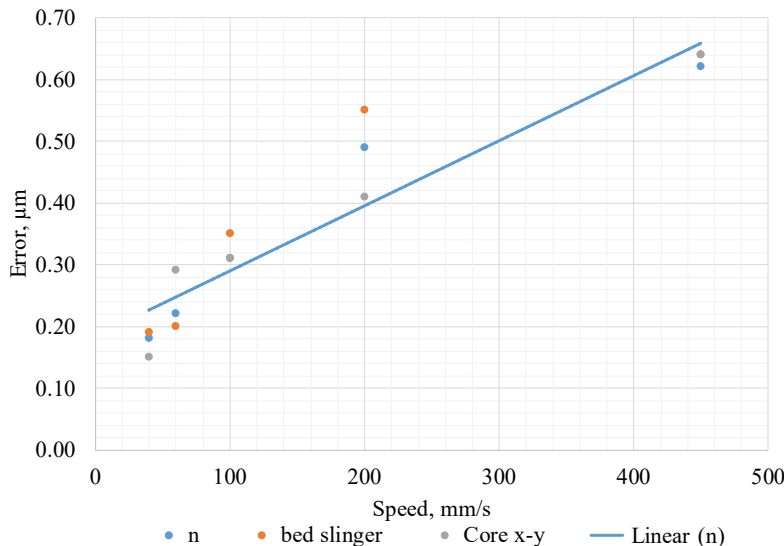
Fig. 19. Change in the filament laying error χ depending on the speed of bypassing the contour

Attention is drawn to the conditionality of the tensile strength of printed elements (σ_{xy} and σ_z) depending on parameter ρ. Based on empirical data, plots of the dependence of strength in the XOY plane (Fig. 20, a) and along the OZ axis (Fig. 20, b) were constructed, which illustrate the practically linear nature of the increase in strength with increasing density ρ in the range of values 0.8...0.98.

The corresponding regression equations are given below:

$$\sigma_{xy} = -0.1106 + 0.8957 \cdot \rho,\tag{16}$$

$$\sigma_z = -0.2914 + 0.8778 \cdot \rho.\tag{17}$$

Studies have shown that there is a significant discrepancy between the strength in the vertical direction OZ and in the horizontal direction XOY (in the filament laying plane), which confirms the anisotropy of article properties when reproduced by conventional 3D printers.

At the same time, the strength of the finished article as a function of the filament laying density coefficient ρ is less than the strength of the filament as a whole by 20...40%, despite the fact that it increases almost linearly when printing denser workpieces.

The problem of filament laying was also considered from the perspective of slicing – the process of dividing the workpiece into layers and providing the necessary movements with the contour. This process also involves additional functions: defining contours, filling conditions, working on consoles, establishing the minimum influence of variable temperatures of base T_s and extruder T_e, etc. Attention was paid to the use of the most modern slicers, in particular Simplify 3D and Creality Print. The latter quite effectively performed the division of the model for printing overhanging elements; Fig. 21.
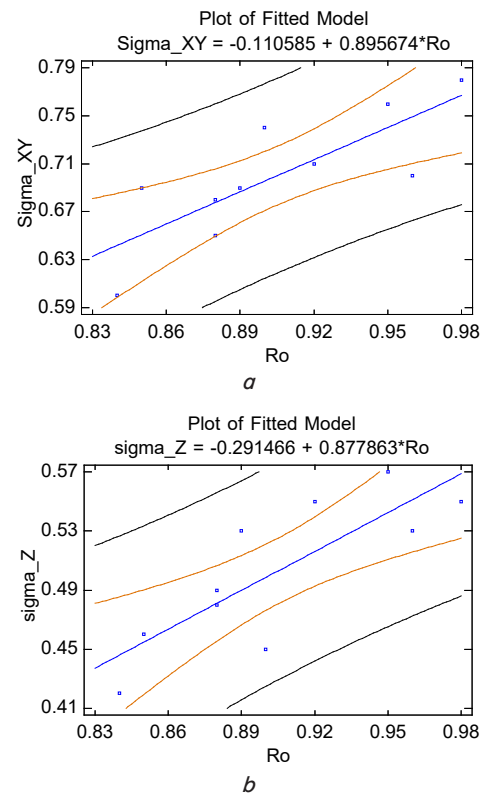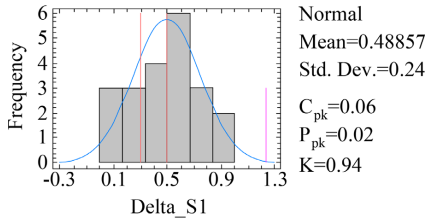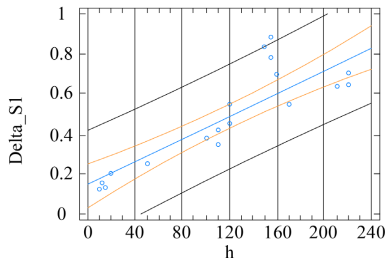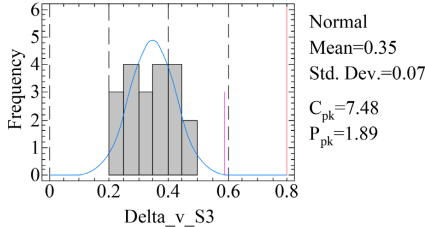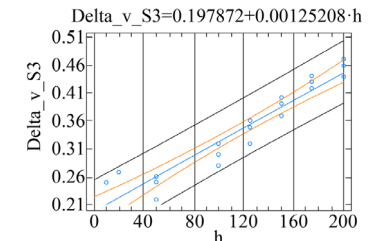

Fig. 20. Dependence of tensile strength σ_{xy} and σ_z on the filament density coefficient ρ: a — in the XOY plane; b — along the vertical Z

Since the corresponding theoretical generalizations of the results of the software package are extremely complicated, these studies were replaced by full-scale experiments. For greater reliability of our results, a certain number of prints of honeycomb models were performed, which allowed us to clarify the classification features of the defects proposed by [27] and reduce them to three groups, according to the cause-and-effect diagram shown in Fig. 6.

Table 7

Statistical processing of modeling results

| No.	Testing the statistical hypothesis about the normal distribution	Regression models
$\chi = f(H)$ for low speeds ($s_k = 35$ mm/s)	**Process Capability for Delta_S1** Nominal=0.3; USL=0.5 Normal Mean=0.48857 Std. Dev.=0.24 C_{pk}=0.06 P_{pk}=0.02 K=0.94	**Plot of Fitted Model** Delta_v_S1=0.139318+0.00289095·h
	All data can be attributed to one general population. It can be said that the simulation does not reveal a statistically significant linear effect of the distance from the table surface to the laying plane H on the controlled error parameter χ. This situation is associated with a critical outlier of values for $H = 180...200$ mm, although the tendency to increase χ with increasing H remains	Correlation coefficient = 0.87292. R-squared = 76.1989 percent. R-squared (adjusted for d.f.) = 74.9462 percent. Standard error of est. = 0.123119. Mean absolute error = 0.0892357. Durbin-Watson statistic = 0.561211 (P = 0.0000). Lag 1 residual autocorrelation = 0.705506
For significant speeds $\chi = f\left(\dfrac{dy_6}{dt}\right) = f(v_6)$ ($s_k = 200$ and 500 mm/s)	**Process Capability for Delta_v_S3** USL=0.8 Normal Mean=0.35 Std. Dev.=0.07 C_{pk}=7.48 P_{pk}=1.89	**Plot of Fitted Model** Delta_v_S3=0.197872+0.00125208·h
	The test was performed using the ω-criterion and the d-criterion for small samples, $10 \leq N < 50$: $$\bar{d} = \frac{1}{nS}\sum_{i=1}^{N}(x_i - \bar{x}),$$ by selected level of significance $\alpha \leq \alpha_1 + \alpha_{11}$ for $q_1(\alpha_1)$ and $q_2(\alpha_2)$. The hypothesis of normality of the distribution of the sample values is rejected; therefore, there is a functional conditionality for the influence of speed $v_6 = s_k$ on error value χ	Correlation coefficient = 0.952654. R-squared = 90.755 percent. R-squared (adjusted for d.f.) = 90.2414 percent. Standard error of est. = 0.0247431. Mean absolute error = 0.0183406. Durbin-Watson statistic = 1.6923 (P = 0.1679). Lag 1 residual autocorrelation = 0.0764491
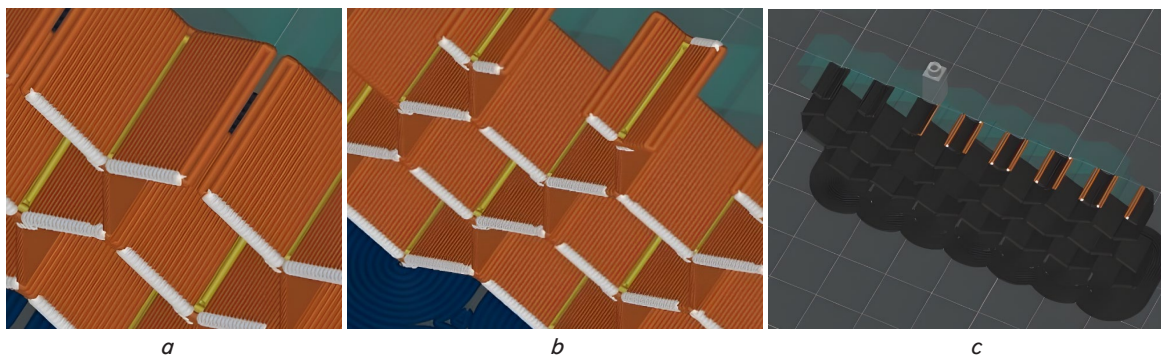
Fig. 21. Formation of inclined walls: *a* — cantilevered transverse filament laying; *b* — basal; *c* — vertical wall building in Creality Print slices

The printed honeycombs were weighed, Fig. 22, *a*, and thicknesses δ_{ci}, mm, were measured on the main planes of the honeycomb: two vertical walls and 4 cantilever, in two mutually perpendicular sections of the vertical plane of the honeycomb; the measurement scheme is in Fig. 22, *b*. The measurements were duplicated 10 times; as a result, a sample of observations in the amount of 120 measurements was obtained. Weighing allowed us to estimate the plastic consumption and the stability of the laying process. It was found that the weight of almost all printed articles was 72 g, with the dispersion of this parameter within 6.1 g.

The results of statistical processing are shown in Fig. 23. The honeycomb itself was cut before measurements to avoid complications in installing the tool.
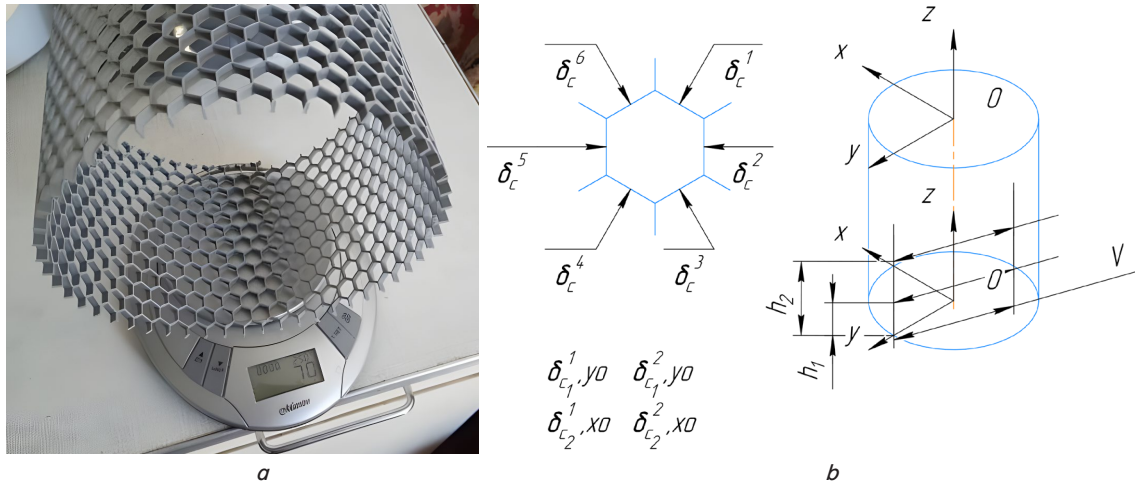
Fig. 22. Determining the parameters of a finished article: a — weighing of cylindrical honeycombs; b — scheme of measurements of the geometric parameters of the cells
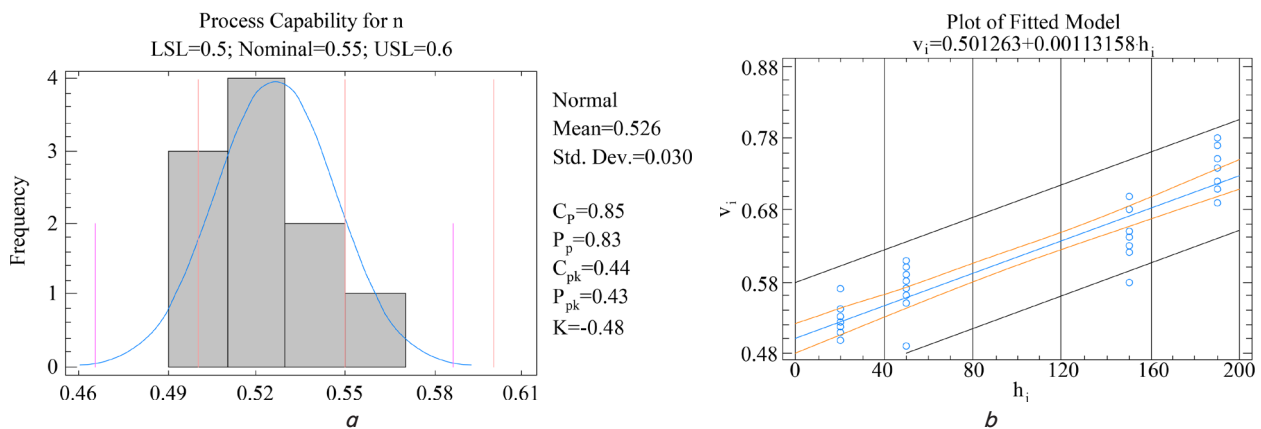

Fig. 23. Results of statistical processing of measurements: a — statistical scattering field; b — postulated regression line for the thickness of the vertical wall $\delta_c^2, \delta_c^5, (k_i)$

The diagram in Fig. 23, a, shows that in general the sample of values of measured honeycomb thicknesses for individual elements can be attributed to a certain general population, in which vertical walls δ_{c2} and δ_{c5} obey the law of normal distribution with practically the same parameters $M(\delta_{c2,5})$ and $\sigma(\delta_{c2,5})$. The same can be said about elements 1, 3, 4 and 6. However, the dispersions are heterogeneous and have a significant difference, i.e., $\sigma(\delta_{c2,5}) \neq \sigma(\delta_{c1,3,4,6})$. Parameters M are also different: $M(\delta_{c2,5}) \neq M(\delta_{c1,3,4,6})$.

If these results can be explained by the fact that the formation of inclined walls is a process with a significant number of random factors and is dynamically unstable, then the difference in the corresponding averaged dispersions σ_j in the function of the increase in the measurement height h_1–h_5 proves that the limited rigidity of an article leads to the occurrence of a greater shift of the layers during laying, and the shape errors become increasingly significant; Fig. 23, b.

Performing a regression analysis made it possible to establish a certain functional conditionality for the change in average thickness δ_{ci} and dispersion $\sigma(\delta_{ci})$. It is shown that an increase in the height of the reproduced model leads to a change in these parameters. In this case, the installation of additional supports in the form of supports of the tree structure is expedient and justified, Fig. 24, since additional supports increase the rigidity of the system as a whole.

Accordingly, the regression models of dependence of the thickness of vertical walls δ_c^5, (k_i) and inclined walls

$\delta_c^2, \delta_c^5, (v_i)$ as a function of height h_i (correlation coefficient not worse than 0.82) are as follows: $k_i = 0.72 + 0.0008 \cdot h_i$, $v_i = 0.50 + 0.001 \cdot h_i$.
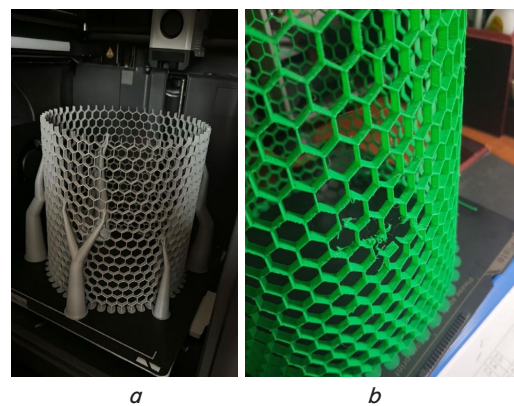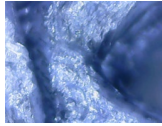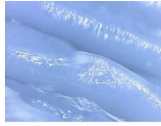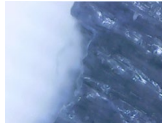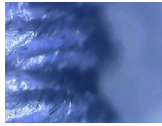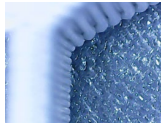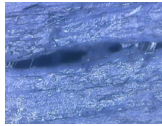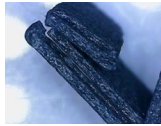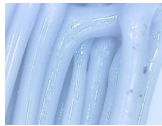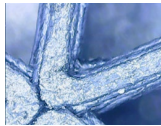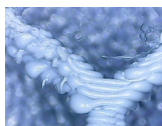

Fig. 24. Implementation of cellular non-rigid systems: a — with intermediate supports-dendrites; b — emergence of defects in the case when such supports are absent

5. 3. Systemizing the defects in 3D printing of honeycomb articles based on experimental studies

The production of a batch of typical honeycomb blanks also allowed us to clarify the typification of defects, which, taking into account [27], are given in Table 8.

Table 8

Defects and errors in printed articles that emerged during the production of sample batches

Type	Classification feature	Example (microphoto)	Type	Classification feature	Example (microphoto)
D_1 – shrinkage	K_0, K_2		D_8 – excessive extrusion	K_0, K_2	
D_2 – deformation	K_0, K_2		D_9 – under-extrusion	K_0, K_2	
D_3 – shift	K_0, K_1, K_2		D_{10} – streaking	K_0, K_1	
D_4 – delamination	K_0, K_2		D_{11} – cracks	K_0, K_1, K_2	
D_5 – twisting	K_0, K_2		D_{12} – clots	K_0	
D_6 – gaps	K_1, K_2		D_{13} – voids	K_0, K_1, K_2	
D_7 – threads outside	K_1, K_2		D_{14} – microscopic foreign inclusions	K_1, K_2	

Given the cause of defects and their conditionality, they were classified into three groups:

– group 1; caused by internal stresses (D_1, D_2, D_4, D_5, D_{11});

– group 2; caused by the dynamic properties of the printer itself (D_3, D_6, D_7);

– finally, group 3 that depends on extrusion conditions (D_8, D_9, D_{10}, D_{12}, D_{13}).

An analysis of defects that occurred during the printing process was performed and summarized in Table 8. The systematization was formed on the basis of classification features K_1–K_3 [27] and typification of defects D_1–D_{13}. At the same time, based on [28], defects were classified by geometric size (K_0), spatial topology (K_1), nature of occurrence (K_2) and location (K_3).

In general, it should be noted that the most dangerous were shrinkage defects D_1 and the occurrence of internal cracks D_{11}, which under certain circumstances (small adhesion area) could cause delamination of article elements D_4.

A conclusion was drawn regarding the additional introduction of a new classification feature D_{14} – microscopic inclusions in the structure of the material. Such inclusions have a significant impact, and their appearance is caused by the presence of moisture and dirt, foreign substances on the surface of the plastic, etc.

Actually, these defects are mutually conditioned, which requires their further clarification and adjustments to the classification. The defect in the form of a shift of layers D_3 was quite easily eliminated by appropriate adjustment of the movements of the printer's working head, in particular, by reducing dynamic loads, defects D_6–D_9 are associated with the extrusion process and can be reduced by appropriate adjustment of the printer's operating conditions.

Defects D_{12}–D_{13} require a detailed analysis of the traceology, which is determined by the slicer used. The transition to new types of slicers reduces such defects.

Microphotographs of honeycomb elements in Fig. 25 showed the following.

At the stage of manufacturing sample honeycombs, the thin-wall search option was used, and printing was performed on a high-speed Bambu Lab K1S printer. Microphotographs of the resulting articles showed that, despite the better geometric parameters of the created honeycombs, their laying density still remained relatively low; increasing the laying density caused a sharp increase in the number of defects and made printing impossible in general. Individual fragments of the honeycomb walls had areas of both unsatisfactory density, Fig. 26; and areas of solid defects, Fig. 27. Such defects were the result of a positioning error when the subsequent laying of the filament after the previous one took place without a base, practically in the air; further laying disrupted the reproduction process, and the plastic simply froze in an arbitrary position. However, further printing could be resumed when the traceology was changed.
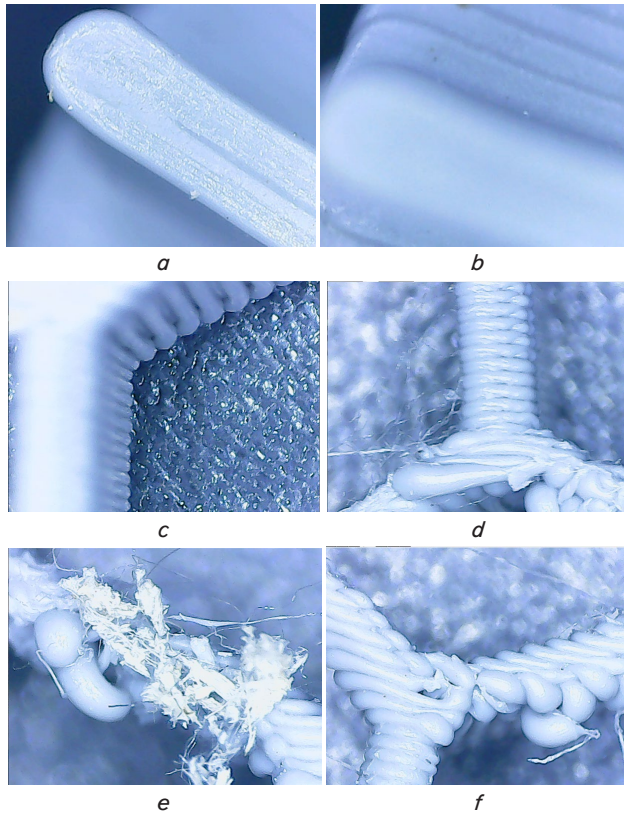
Fig. 25. Microphotographs (x250) of fragments of the printed article: *a* — two-thread wall; *b* — cantilever elements; *c* — growth of the interlayer defect; *d* — formation of the defective layer; *e* — phantom parts; *f* — plastic sludge on the ends
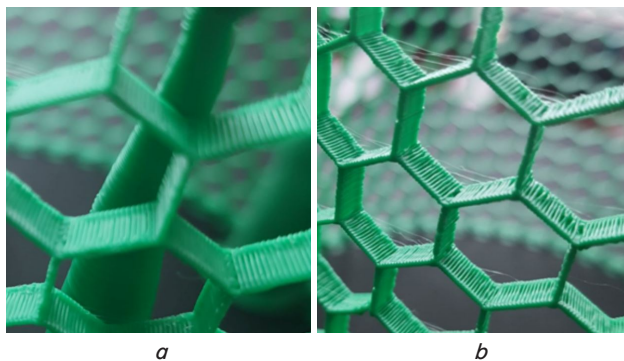

Fig. 26. Macrophotograph (x15) of parts of a honeycomb designed with overhanging elements: *a* — without intermediate supports; *b* — with additional means of support
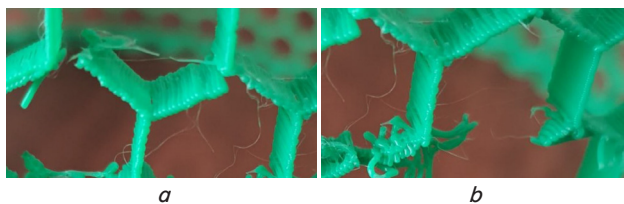

Fig. 27. Solid defects: *a* — rupture of the honeycomb wall; *b* — damage to a single element as a whole

At the same time, it should be noted that increasing the stiffness of the model by introducing additional supports not only reduces the probability of failure but also improves the quality of layering; Fig. 26, *b*.

The problems that arise turned out to be identical for both unreinforced and reinforced materials.

5. 4. Mathematical model of FDM printing process reliability and predictability of article properties

Since the number of manufactured honeycomb samples is quite limited (6 samples were manufactured, including 1 sample from PLA-C, as well as one sample with an outer wall), statistical data processing was extremely difficult to perform. That is why a microscopic study of sections and honeycomb elements was performed, which had similar and comparable characteristics regarding the extruder passage paths, the density of the layout, and the speed of model reproduction.

Statistical data processing regarding the dependence of χ, and, accordingly, ρ provided that $\rho = f(\chi)$ showed the following: the use of Bed Slinger printers at contour bypass speeds $s_k = 50...75$ mm/s is ineffective; the errors are non-systematic, which is proven by Table 9. Thus, the determined values of density ρ can be attributed to a certain general population, in which this parameter ρ (as well as χ) obeys the law of normal distribution for the entire range of H values with the corresponding group $M(\rho_{Hi})$ and $\sigma(\rho_{Hi})$. For printers of the Core X–Y type, the functional relationship is obvious; therefore, the prediction of the parameters of the finished article is effective and significant.

The bottom line of Table 9 proves that at certain heights $H = H_{kr}$ the dynamic properties of the model and the elastic system of the printer manifest, which leads to a resonant increase in χ. This situation confirms the possibility of the defects shown in Fig. 26, 27, and requires the introduction of additional means for ensuring the rigidity of the structure into the design. For a honeycomb with geometric parameters shown in Fig. 10, this is height $H = 150...185$ mm; however, the functional conditionality for the second type of articles will be different.

Our studies have shown that based on the considered model of loss of functional properties of the shell (5), it is possible to propose a model of reliability for printing the non-rigid honeycombs, which is based on (4) and whose components will be as follows:

$$P_v(t) \cong P_v(H) = 1 - \left[0.5 + \Phi\left(\frac{\rho - \gamma_\rho H}{\sqrt{\sigma_\rho^2 + \sigma_{y\rho}^2 H}} \right) \right],$$

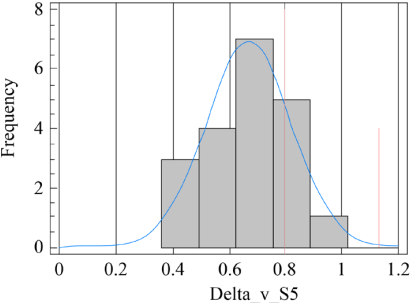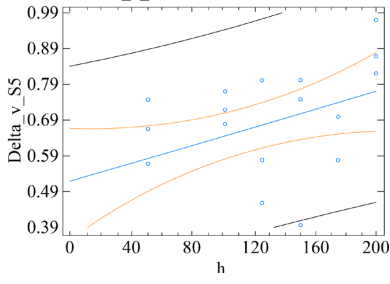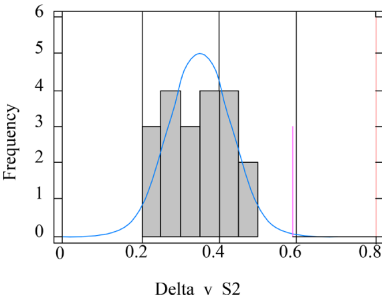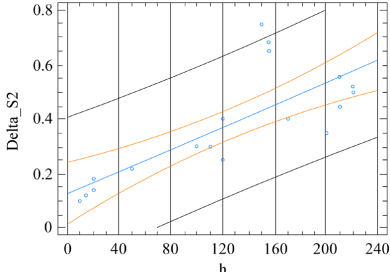$$P_f(t) = e^{-\lambda_f fT}, \ P_a(t) = e^{-\lambda_a T}, \tag{18}$$

where $P_v(t)$ is the probability of violation of the conditions of laying and solidification of the plastic, which increases with increasing height of the laid layer H, mm, in the first approximation linearly; $P_f(t)$ – probability of failures during filament feeding as a flow of possible failures in the form of lack of power supply (not automatically restored, nozzle clogging, change in filament diameter, which led to the formation of plugs in the feed channel, as a function of time t; $P_a(t)$ – probability of violation of adhesive adhesion conditions with the base – as a flow of failures (sudden) in the form of destruction of the bond with the base, as a function of time t.

Since the height of an article H is also a function of time, if necessary, the wool can be represented as $H = f(t)$. The manifestation of sudden failures (Fig. 27, *a*) simultaneously with gradual ones corresponds to the components in (3). Going beyond the expected values of the initial quality indicators by parameter X, where X is, for example ρ, which functionally determines $[\sigma]_{x,y,z}$, will correspond to Fig. 28.

Table 9

Statistical analysis of experimental results from Bed Slinger and Core X-Y printers

| No.	Testing the statistical hypothesis about the normal distribution	Regression models
$\chi = f(H)$ for low speeds ($S_k = 35$ mm/s), printer Bed Slinger	**Process Capability for Delta_v_S5** USL=0.8 Normal Mean=0.673 Std. Dev.=0.030 C_{pk}=0.37 P_{pk}=0.27	**Plot of Fitted Model** Delta_v_S5=0.520588+0.00125853·h
	All data can be attributed to one general population. It can be said that the measured values of errors practically do not depend on the height of the reproduced model H; at the same time, a certain tendency to increase is observed. It is difficult to build a reliability model, since the measured data have more dispersion within the group than the expected change under the influence of the controlled factor	Correlation Coefficient = 0.492146. R-squared = 24.2207 percent. R-squared (adjusted for d.f.) = 20.0108 percent. Standard error of est. = 0.137832. Mean absolute error = 0.108012. Durbin-Watson statistic = 1.38979 (P = 0.0457). Lag 1 residual autocorrelation = 0.261177
$\chi = f(H)$ for significant speeds ($S_k = 200$ and 500 m/s)	**Process Capability for Delta_v_S5** USL=0.8 Normal Mean=0.35 Std. Dev.=0 C_{pk}=7.48 P_{pk}=1.89	**Plot of Fitted Model** Delta_v_S2=0.129873+0.00200342·h
	The test was performed using the ω-criterion and the d-criterion for small samples, $10 \le N < 50$ $$\bar{d} = \frac{1}{nS}\sum_{i=1}^{N}(x_i - \bar{x})$$ by the selected level of significance $\alpha \le \alpha_1 + \alpha_{11}$ for $q_1(\alpha_1)$ and $q_2(\alpha_2)$. The hypothesis of normal distribution of the sample values is rejected; therefore, there is a functional conditionality for the influence of speed $\chi\chi = f(H)$ on error value χ	Correlation coefficient = 0.781238. R-squared = 61.0333 percent. R-squared (adjusted for d.f.) = 58.9824 percent. Standard error of est. = 0.121982. Mean absolute error = 0.0770081. Durbin-Watson statistic = 0.837281 (P = 0.0005). Lag 1 residual autocorrelation = 0.568133. The existing peak is due to the dynamic properties of the reproduction system
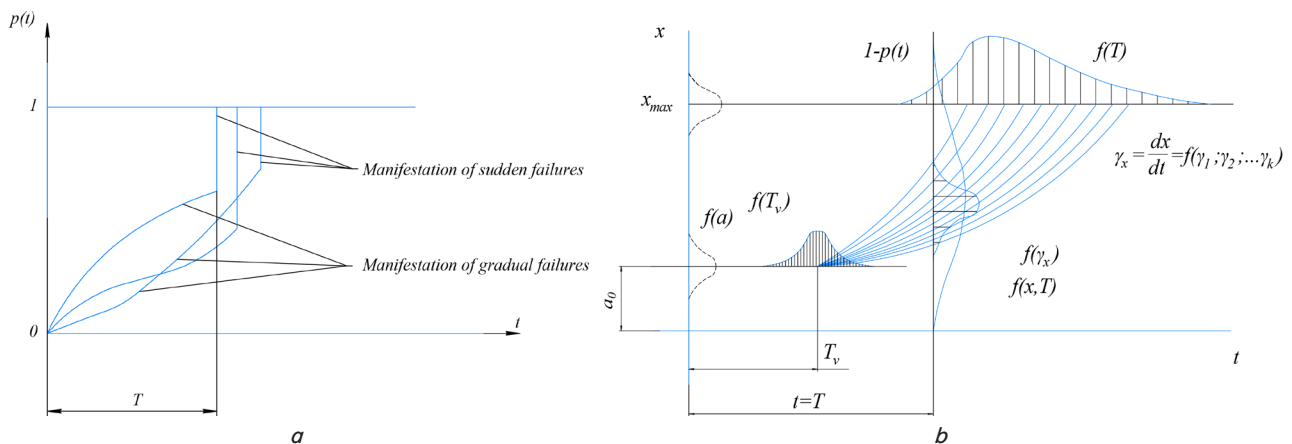
Fig. 28. Emergence of sudden and gradual failures:
a − during 3D printing; *b* − defect formation during process disturbances

When theoretically calculating ρ, it is possible to predict additional plastic consumption in the event of printing errors or changes in printing conditions to ensure the required parameters, in particular, $[\sigma]_{x,y,z}$.

6. Discussion of results based on investigating the reproduction of a test honeycomb article

Modern FDM printers, despite the difference in designs, are capable of printing honeycombs. However, different technical solutions cope with the task in different ways.

For high-speed Core XY printers with a table moving along the vertical coordinate (Table 4, last line), there is a possibility of local defects associated with a change in the contour path, leading to local short-term disturbances in the system. In this case, the speed of bypassing the contour can reach 200–300 mm/s with a total error of no more than 0.5 mm at height $H = 200$ mm; Fig. 12, 13. This is confirmed by individual defects, Fig. 25, c, which generally do not have catastrophic consequences and do not lead to violations of the honeycomb structure (Fig. 27).

For Bed Slinger printers, defects of almost all types can occur maximally on the upper layers of the contour, while the bypass speed has a prevailing influence, and to eliminate defects, in particular (Fig. 25), it should not exceed 35…50 mm/s. The problem of dynamic deformation of the article during table movement is significant, which causes displacement of the filament laying points, which can lead to the impossibility of the layer joining process due to a sharp deterioration in the density of the laid material. The latter statement is also consistent with the results of SSS of a non-rigid honeycomb blank, Fig. 18, according to which there are possible cases when the displacement of the next layer relative to the previous one will be critical and structural violations will occur in accordance with Fig. 25, d, e, with the loss of part of the honeycomb (Fig. 27).

Since the honeycomb structure is not rigid, with many cantilever elements, the extrusion of the material is extremely complicated. Even in the initial layers, defects in the form of shifts, partitions, and loss of cantilever elements located at an angle are quite often formed (Fig. 25, b).

At the same time, the involvement of additional supports in the form of tree-like structures (Fig. 26, b) improves the reliability of the process, precedes the separation of the workpiece from the base, and improves the geometric accuracy of the article, contributes to an increase in the level of model reproducibility regardless of the type of printer.

Our studies have shown that the probability of disturbances in the steady state of the technological process is maximum with the simultaneous action of inertial forces and forces from the extruder, which are proportional to the printing speed. That is why the increase in the rigidity of the honeycomb system should be carried out in the plane of the smallest stiffness profile, and printing should be carried out at a low speed; Fig. 19; equations (14), (15).

It should be noted that it was not always possible to create a thin wall when printing a cylindrical honeycomb. Usually, the wall grew satisfactorily in the vertical direction, but all inclined walls, due to their small thickness, delaminate and fall off (Fig. 25, e). Disabling the option to search for thin walls (Fig. 25, a) from the slicer involved laying out the wall in two threads (the thread thickness was 0.38…0.42 mm, the wall was 0.5 mm, and the program formed thicker walls). As a result, a satisfactory cross-section was obtained (Fig. 25, c),

but the subsequent formation of the layer (Fig. 25, d, e) occurred with an increase in thickness to 1.2…1.5 mm, and with the formation of defects, phantom parts (Fig. 25, f) and plastic sludge at the ends (Fig. 25, e).

For this purpose, a limitation of the filament laying speeds at the points of change in direction of movement with a limitation of accelerations was applied, and it was also proposed to compensate for the increase in the height of the honeycomb by installing additional supports so that they were located in the plane of minimum stiffness.

Despite the difference in the printers used, in general, all articles corresponded to the accuracy of reproduction of elements according to IT11…IT9, which is acceptable for engineering applications. However, the dynamic properties of the printers and the limited rigidity of the workpiece significantly influenced the printing reliability model, (18): for Core XY printers, the reproduction of the test honeycomb occurred with the provision of predicted mechanical properties at the level of 95 %, for Bed Slinger – 45…68 %. The latter was manifested by the possibility of obtaining one suitable article with two or three defective ones.

The assumption regarding the connection of ρ with the expected mechanical properties, in particular, the tensile strength σ_{xy} and σ_z (Fig. 20), equations (16), (17) is also confirmed. Therefore, the parameter ρ, established by (6) or experimentally measured for two sections, as well as its change in the function of H, $\rho = f(H)$, can uniquely determine the probability $P_v(t)$, (12), and $P(t)$ in general (by (4)) (Fig. 27, b).

Therefore, to assess the probability of reliable reproduction of honeycombs during FDM printing on ordinary printers (2), it is advisable to use the reliability model (18) identified for a specific printer with the following parameters:

– γ_ρ is the rate of change in the density of plastic deposition (can be established on the basis of optical or microelectronic studies of the structure of the deposited filament on some sections of the reproduced model;

– H is the key geometric parameter of the model (in particular, for most articles this is the height of the model, i.e., the distance from the base of the deposition to the highest point of the model, mm);

– σ_ρ^2, $\sigma_{\gamma\rho}^2$ – scattering of actual values of density ρ (at the beginning of plastic laying) and rate of change of density γ_ρ, respectively; λ_f – failure rate associated with filament defects and λ_a – failure rate associated with adhesion violation to the base (sudden). Parameters λ_f and λ_a are determined based on statistical observations of the printing process of similar articles.

Several important provisions can be stated regarding reliable printing of complex shell articles:

– printing should take place using sacrificial elements, which with minimal material consumption provide maximum printing rigidity; as a result, minimal dynamic displacements χ of interlayer adhesion areas and stability of mechanical properties of the article are ensured;

– support areas should be such as to provide the required values of adhesive adhesion of the model to the base; at the same time, the larger the solid base, the greater the probability of its warping due to the arising residual stresses;

– the plastic deposition density parameter ρ correlates satisfactorily with the probability of reliable printing of the shell article and can be an argument for the reliability function. A higher deposition density makes the process more reliable. In addition, this parameter also determines the expected mechanical properties of the finished article.

Comparison of microphotographic samples of the deposited walls, defect formation zones (mainly at sharp corners of

the contour bypass) proves that the use of reinforced material, working with slightly higher extrusion temperatures makes it possible to significantly improve both the density of the filament deposition (with a corresponding increase in the adhesion plane) and avoid a number of defects inherent in articles made of unreinforced materials. Thus, further research should be aimed at identifying the patterns of formation of interlayer and interfiber adhesion planes according to the scheme in Fig. 9.

It should also be noted that the proposed approach has certain limitations due to the fact that the parameters of the reliability model are determined directly by the dynamic system of the printer, and for different types, different materials used, different printing modes may differ significantly. Therefore, despite the general conditionality, they require refinement for specific conditions.

7. Conclusions

1. A simulation modeling of the dynamic printer system has been performed, which takes into account the peculiarities of the formation of adhesive bonding planes both between the filaments and between the layers; the flow of the extrudate was estimated and it was shown that dynamic disturbances in the form of self-oscillations or forced oscillations can cause the appearance of a dynamic error c, which under the conditions of forming thin walls (such as honeycomb walls) can lead to a significant increase in printing defects. As a result, the mechanical properties will decrease by the value $k_{x,y,z} = 0.35...0.85$; $[\sigma]_x = k_x\sigma_t$; $[\sigma]_y = k_y\sigma_t$; $[\sigma]_z = k_z\sigma_t$. Since the occurrence of dynamic disturbances is a random process, an assumption was made about the feasibility of using a process reliability model to predict the mechanical properties of articles.

2. Based on the SSS analysis of a workpiece located on the moving table of the printer, the features of printing non-rigid honeycombs were taken into account. High honeycomb systems are prone to loss of stability during reproduction and must be printed by involving additional support means (for example, dendritic support elements). During planar filament laying, a significant number of defects are formed, which it is desirable to take into account when determining the basic mechanical properties of article material during its static and dynamic force analysis. It was also established that the expected mechanical properties, in particular, $[\sigma]_{x,y,z}$, are determined by the process conditions, dynamic phenomena in the elastic system of the printer, formed by adhesive bonds of the extrudate elements, and depend directly on the density of the laying.

3. Parametric failures and printing defects that arise have been systematized. The classification of defects was clarified; it is proposed adding D14 to the classifier – microscopic foreign inclusions, which are quite often the focus of defects during working loads. It is shown that the main defect that leads to a significant disruption of the normal course of the process is dynamic errors in the positioning of the extruder, consistent with the process of extrusion of the filament melt. It has also been shown

that the density of filament laying, which is proposed to be denoted ρ, determines the strength parameters of the finished article (since it is functionally related to them), and also satisfactorily correlates with the probability of reliable printing of shell article, and can be an argument for the reliability function.

4. Reliability models have been proposed that describe the occurrence of parametric, gradual (as a result of slowly occurring processes), and functional, sudden (violation of adhesion conditions and problems with the filament) failures. It is shown that printers of different designs have different reliability in terms of honeycomb reproduction: for Core XY printers, the reproduction of the test honeycomb occurred with the provision of predicted mechanical properties at the level of 95 %, for Bed Slinger – 45...68 %.

The basics of ensuring the predicted properties of the honeycomb filler obtained by additive processes, in particular, FDM printing, have been formulated. Thus, algorithmically, it is necessary to provide for limitations on the filament laying speeds at points of change in direction of movement with acceleration limitations, to ensure the movement of the extruder along long routes; technically – to take into account the height of the honeycomb and install additional supports so that they are located in the plane of minimum rigidity.

In general, under the conditions of generation and rational placement of supports, the printing results will be satisfactory: the accuracy of the basic dimensions of the article is ensured no worse than 11...12 quality, and the thickness of the honeycomb walls is determined by the filament laying modes and is generally equal to no less than 1.5 diameters of the nozzle used. At the same time, no significant differences in quality indicators between reinforced and unreinforced plastic were observed.

Conflicts of interest

The authors declare that they have no conflicts of interest in relation to the current study, including financial, personal, authorship, or any other, that could affect the study, as well as the results reported in this paper.

Funding

The study was conducted without financial support.

Data availability

The data will be provided upon reasonable request.

Use of artificial intelligence

The authors confirm that they did not use artificial intelligence technologies when creating the current work.

References

1. Castanie, B., Bouvet, C., Ginot, M. (2020). Review of composite sandwich structure in aeronautic applications. Composites Part C: Open Access, 1, 100004. https://doi.org/10.1016/j.jcomc.2020.100004
2. Ashraf, W., Ishak, M. R., M. Y. M., Z., Yidris, N., Ya'Acob, A. M. (2021). Investigation of Mechanical Properties of Honeycomb Sandwich Structure with Kenaf/glass Hybrid Composite Facesheet. Journal of Natural Fibers, 19 (13), 4923–4937. https://doi.org/10.1080/15440478.2020.1870637

3. Gill, E., D'Amico, S., Montenbruck, O. (2007). Autonomous Formation Flying for the PRISMA Mission. Journal of Spacecraft and Rockets, 44 (3), 671–681. https://doi.org/10.2514/1.23015

4. Bollen, P., Quiévy, N., Bailly, C., Huynen, I., Pardoen, T. (2014). Multifunctional sandwich structure for electromagnetic absorption and mechanical performances. 16th European Conference on Composite Materials (ECCM16).

5. Tian, X., Todoroki, A., Liu, T., Wu, L., Hou, Z., Ueda, M. et al. (2022). 3D Printing of Continuous Fiber Reinforced Polymer Composites: Development, Application, and Prospective. Chinese Journal of Mechanical Engineering: Additive Manufacturing Frontiers, 1 (1), 100016. https://doi.org/10.1016/j.cjmeam.2022.100016

6. Khaleelullah, A., Basha, Sk. J., Rangavittal, H. K. (2012). Design and Analysis of Propellant Tanks Support Structure for an Advanced Spacecraft. International Journal of Applied Research in Mechanical Engineering, 194–200. https://doi.org/10.47893/ijarme.2012.1035

7. Wlodarczyk, P. (2001). Modelarstwo lotnicze i kosmiczne. Warszawa, 384.

8. Chen, Y., Li, T., Jia, Z., Scarpa, F., Yao, C.-W., Wang, L. (2018). 3D printed hierarchical honeycombs with shape integrity under large compressive deformations. Materials & Design, 137, 226–234. https://doi.org/10.1016/j.matdes.2017.10.028

9. Uspensky, B., Derevianko, I., Avramov, K., Polishchuk, O., Salenko, A. (2022). Experimental and Numerical Study on Fatigue of Sandwich Plates with Honeycomb Core Manufactured by Fused Deposition Modelling. Applied Composite Materials, 29 (5), 2033–2061. https://doi.org/10.1007/s10443-022-10057-w

10. Comparing properties of FDM, SLS and resin 3D-printing plastics. Available at: https://www.liqcreate.com/supportarticles/properties-fdm-sls-resin/

11. Caulfield, B., McHugh, P. E., Lohfeld, S. (2007). Dependence of mechanical properties of polyamide components on build parameters in the SLS process. Journal of Materials Processing Technology, 182 (1-3), 477–488. https://doi.org/10.1016/j.jmatprotec.2006.09.007

12. Popov, V. V., Fleisher, A. (2020). Hybrid additive manufacturing of steels and alloys. Manufacturing Review, 7, 6. https://doi.org/10.1051/mfreview/2020005

13. Barnatt, C. (2016). 3D Printing. CreateSpace Independent Publishing Platform, 318.

14. Salenko, A., Kostenko, A., Tsurkan, D., Zinchuk, A., Zagirnyak, M., Orel, V. et al. (2023). A New FDM Printer Concept for Printing Cylindrical Workpieces. Information Technology for Education, Science, and Technics, 459–483. https://doi.org/10.1007/978-3-031-35467-0_28

15. Salenko, O., Derevianko, I., Samusenko, O., Avramov, K., Lithot, O., Rogulin, V. (2021). Creation of sealed strong structures of rocket and space equipment FDM printing methods by ULTEM ™ 9085 PEI plastic. Mechanics and Advanced Technologies, 5 (3), 282–293. https://doi.org/10.20535/2521-1943.2021.5.3.246626

16. Salenko, A., Melnychuk, P., Lashko, E., Chencheva, O., Titarenko, O., Derevianko, I., Samusenko, A. (2020). Ensuring the functional properties of responsible structural plastic elements by means of 3-D printing. Eastern-European Journal of Enterprise Technologies, 5 (1 (107)), 18–28. https://doi.org/10.15587/1729-4061.2020.211752

17. Derevianko, I. I., Avramov, K. V., Uspenskyi, B. V., Salenko, O. F. (2024). Manufacturing Technology, Experimental and Numerical Analysis of Static Bending of Three-Layer Composite Plate with Honeycomb Structure. Journal of Mechanical Engineering, 27 (3), 25–33. https://doi.org/10.15407/pmach2024.03.025

18. Bobyr, M. I., Kryshchuk, M. G., Salenko, O. F., Onyshchenko, E. E., Tsurkan, D. O., Kostenko, A. O. et al. (2024). Damage Development in a Cellular Axisymmetric Tank Additive-Manufactured from Plastic Filament. Part 1. Damage Development in Cellular Axisymmetric Multilayer Shells Under Critical Mechanical Loads and Quivalent Properties of Model Layers for Stress-Strain State Estimation. Strength of Materials, 56 (3), 484–499. https://doi.org/10.1007/s11223-024-00664-2

19. Chieng, B. W., Ibrahim, N. A., Then, Y. Y., Loo, Y. Y. (2016). Mechanical, thermal, and morphology properties of poly(lactic acid) plasticized with poly(ethylene glycol) and epoxidized palm oil hybrid plasticizer. Polymer Engineering & Science, 56 (10), 1169–1174. https://doi.org/10.1002/pen.24350

20. Matsuzaki, R., Ueda, M., Namiki, M., Jeong, T.-K., Asahara, H., Horiguchi, K. et al. (2016). Three-dimensional printing of continuous-fiber composites by in-nozzle impregnation. Scientific Reports, 6 (1). https://doi.org/10.1038/srep23058

21. Schuldt, S. J., Jagoda, J. A., Hoisington, A. J., Delorit, J. D. (2021). A systematic review and analysis of the viability of 3D-printed construction in remote environments. Automation in Construction, 125, 103642. https://doi.org/10.1016/j.autcon.2021.103642

22. Salenko, O., Drahobetskyi, V., Symonova, A., Onishchenko, E., Kostenko, A., Tsurkan, D., Vasiukov, D. (2024). Damage Behavior of Multilayer Axisymmetric Shells Obtained by the FDM Method. Journal of Engineering Sciences, 11 (1), D27–D35. https://doi.org/10.21272/jes.2024.11(1).d4

23. Zagirnyak, M., Salenko, O., Alnusirat, W., Golovko, L., Orel, V., Kulynych, V. (2024). Increasing the Strength of Thin-walled Products Obtained by FDM Using the Thin Surface Films. Przeglad Elektrotechniczny, 3, 289–292. https://doi.org/10.15199/48.2024.03.52

24. Derevianko, I., Avramov, K., Uspensky, B., Salenko, A. (2021). Experimental analysis of the mechanical characteristics of launch vehicle parts manufactured by FDM additive technologies. Technical Mechanics, 1, 92–100. https://doi.org/10.15407/itm2021.01.092

25. Kuzmych, L. V. (2021). Mechanical impacts on the reliability of complex technical systems. Technical Sciences and Technologies, 4 (14), 28–33. https://doi.org/10.25140/2411-5363-2018-4(14)-28-33

26. Yakovyna, V., Matseliukh, V. (2017). Ohliad i analiz modelei nadiynosti prohramnoho zabezpechennia. Visnyk Natsionalnoho universytetu "Lvivska politekhnika". Kompiuterni nauky ta informatsiyni tekhnolohiyi, 864, 130–140. Available at: http://nbuv.gov.ua/UJRN/VNULPKNIT_2017_864_19

27. Gordeev, E. G., Galushko, A. S., Ananikov, V. P. (2018). Improvement of quality of 3D printed objects by elimination of microscopic structural defects in fused deposition modeling. PLOS ONE, 13 (6), e0198370. https://doi.org/10.1371/journal.pone.0198370

28. Wu, M., Phoha, V. V., Moon, Y. B., Belman, A. K. (2016). Detecting Malicious Defects in 3D Printing Process Using Machine Learning and Image Classification. Volume 14: Emerging Technologies; Materials: Genetics to Structures; Safety Engineering and Risk Analysis. https://doi.org/10.1115/imece2016-67641